

# Revisiting critical orbits of test particles traveling in a black hole background<sup>a</sup>

Ping Li,<sup>1,2,†</sup> Jun Cheng,<sup>1,2,‡</sup> and Jiang-he Yang<sup>1,3,§</sup>

<sup>1</sup>*College of Mathematics and Physics,  
Hunan University of Arts and Sciences, 3150 Dongting Dadao,  
Changde City, Hunan Province 415000, China*

<sup>2</sup>*Hunan Province Key Laboratory Integration and Optical Manufacturing Technology,  
3150 Dongting Dadao, Changde City, Hunan Province 415000, China*

<sup>3</sup>*Center for Astrophysics, Guangzhou University,  
230 West Ring Road, Guangzhou, Guangdong Province 510006, China*

arXiv:2602.09568v1 [gr-qc] 10 Feb 2026

---

<sup>a</sup> Submitted to Chinese Physics C

# Abstract

This paper systematically revisits the critical orbits of test particles moving in various black hole backgrounds, including Schwarzschild, Reissner–Nordström, Kerr, and Kerr–Newman spacetimes. We identify the critical orbit cases directly from the root structure of the radial equation, and provide explicit expressions relating the relevant parameters—energy, angular momentum, and charge-to-mass ratio—to the critical radius, as well as explicit expressions for the critical orbits in each scenario. Special attention is given to the relationship between the photon spheres, black hole shadows and the critical null geodesics. Extensive numerical results are also provided.

## I. INTRODUCTION

Critical orbits are defined as those trajectories for which the radial kinetic energy function admits either a double or triple real root, corresponding to an unstable circular orbit or motion that neither falls into the black hole nor escapes to infinity. Critical orbits are powerful tools for analytically studying black hole shadows and accretion processes. However, as a specialized subclass of geodesics, they are rarely examined as stand-alone entities in the literature. In some literature, critical orbits may be overlooked in the broader discussion. The primary objective of this paper is to conduct a comprehensive review of the key properties of critical orbits, aiming to renew researchers’ attention toward this significant topic in the field.

The study of geodesic motion in black hole spacetimes has a long history. In spherically symmetric spacetimes, the earliest analytical solution for geodesic motion in Schwarzschild spacetime can be traced back to Droste [1] in 1917. Hagihara conducted a comprehensive classification of all possible test particle motions in Schwarzschild spacetime, and his work [2] has remained a classic reference. In Reissner-Nordström (RN) spacetime, Grunau and Kagramanova [3] provided an analytical solution for the motion of electrically and magnetically charged test particles. Much of this work is built on the foundational theory of Weierstrass elliptic functions, though significant research [4–9] has also been developed using Jacobi elliptic functions and Legendre integrals. In rotating, axisymmetric spacetimes,

---

† [Lip57120@huas.edu.cn](mailto:Lip57120@huas.edu.cn)

‡ [chengjun@huas.edu.cn](mailto:chengjun@huas.edu.cn)

§ [yjianghe@163.com](mailto:yjianghe@163.com)

Carter [10] conducted the first analytical study of geodesics in Kerr spacetime in 1968. In this work, by leveraging the separability of the Hamilton–Jacobi equation for test particles, he identified a conserved quantity now known as the Carter constant. In 2003, Mino [11] introduced the so-called Mino time, which completely decouples the geodesic equations. For more recent literature, see [12–17]. In the case of spacetimes with a cosmological constant, Hackmann et al. performed analytical integrations for Schwarzschild–de Sitter [18, 19] and Reissner–Nordström–de Sitter geometries [20] using hyperelliptic  $\theta$  and  $\sigma$  functions. Similar methods have also been extended to the Kerr–de Sitter spacetime [21]. In addition to the literature mentioned above, a number of books also discuss geodesic motion in black hole spacetimes in considerable detail, e.g. [22–25].

Another important goal of this paper is to lay the groundwork for a 3+1 formalism describing the accretion of a Vlasov gas onto a Kerr–Newman black hole. In 2017, Rioseco and Sarbach [26] developed a modern analytical theory for relativistic collisionless Vlasov gas accretion onto a Schwarzschild black hole. In their model, the tangential pressure exceeds the radial pressure at the horizon [27], offering a partial explanation for the issue of low accretion rates, which has attracted considerable attention. Subsequently, this model was quickly extended to describe accretion onto a moving Schwarzschild [28, 29], Reissner–Nordström [30] and Kerr [31–33] black holes. In a related development, Mach et al. constructed a numerical framework using Monte Carlo methods to simulate the motion of collisionless gas in a Schwarzschild background [34, 35]. Since our focus is on accretion models, we are particularly interested in the scenario where test particles fall toward the black hole from infinity. Similar studies of unbound orbits in Schwarzschild spacetime have already been discussed, see [36, 37]. It should be noted that the accretion of neutral particles onto a black hole does not induce charge evolution. To investigate the effect of accretion on black hole charge, we have recently extended this model to describe the accretion of a collisionless Fermi gas onto a Reissner–Nordström black hole [38].

In the accretion model proposed by Rioseco and Sarbach [26], test particles are assumed to be in thermal equilibrium at infinity. Under gravitational influence, these particles follow geodesics into the finite region. Consequently, they naturally separate into three categories: those that fall into the black hole and are absorbed, those that are scattered by the black hole and return to infinity, and—lying between these two scenarios—a critical case in which particles neither enter the black hole nor escape to infinity, but instead asymptotically

approach an unstable bound orbit. Therefore, examining this critical behavior is essential in accretion theory, as it defines the boundary in parameter space between absorbed and scattered particles. A similar line of reasoning applies to the analysis of the shadow boundary of a black hole. Therefore, this paper provides a systematic review of methods for handling critical geodesics in both spherically symmetric and axisymmetric rotating spacetimes. It aims to enable efficient identification of the relevant parameters associated with critical geodesics and to facilitate their analytical or numerical analysis.

The paper is organized as follows. In section II, we review the derivation of the equations of motion for charged test particles in Kerr–Newman spacetime using the separability of the Hamilton–Jacobi equation. Sections III through VI present a detailed analytical treatment of critical orbits — both null and timelike — in Schwarzschild, Reissner–Nordström, Kerr, and Kerr–Newman black hole spacetimes, respectively. The final section provides conclusions and discussion.

## II. THE GENERAL EQUATIONS OF MOTION

In this section, we provide a review of equations of motions for charged particles traveling in Kerr–Newman black hole. We work in the Boyer–Lindquist coordinates  $(t, r, \theta, \varphi)$ . The Kerr–Newman metric is well-known and can be written as

$$ds^2 = -\frac{\Delta - a^2 \sin^2 \theta}{\rho^2} dt^2 - 2\frac{a \sin^2 \theta (2Mr - Q^2)}{\rho^2} dt d\varphi + \frac{\rho^2}{\Delta} dr^2 + \rho^2 d\theta^2 + \frac{(r^2 + a^2)^2 - \Delta a^2 \sin^2 \theta}{\rho^2} \sin^2 \theta d\varphi^2, \quad (1)$$

where

$$\Delta = r^2 - 2Mr + a^2 + Q^2, \quad (2)$$

$$\rho^2 = r^2 + a^2 \cos^2 \theta, \quad (3)$$

and  $M$  is the mass,  $Q$  is the charge,  $a = J/M$  is the angular momentum per unit mass of the black hole. The outer and inner horizons are the roots of  $\Delta(r) = 0$  and are expressed as

$$r_{\pm} = M \pm \sqrt{M^2 - (a^2 + Q^2)}. \quad (4)$$

Generally, the condition for a black hole to possess an event horizon is given by  $0 \leq a^2 + Q^2 \leq M^2$ . The potentials of electromagnetic fields for the background are  $(-\frac{Qr}{\rho^2}, \frac{Qr}{\rho^2} a \sin^2 \theta, 0, 0)$ .

The inverse metric can be expressed as

$$g^{\mu\nu} = \begin{pmatrix} -\frac{(r^2+a^2)^2-\Delta a^2 \sin^2 \theta}{\rho^2 \Delta} & 0 & 0 & -\frac{a(2Mr-Q^2)}{\rho^2 \Delta} \\ 0 & \frac{\Delta}{\rho^2} & 0 & 0 \\ 0 & 0 & \frac{1}{\rho^2} & 0 \\ -\frac{a(2Mr-Q^2)}{\rho^2 \Delta} & 0 & 0 & \frac{\Delta-a^2 \sin^2 \theta}{\rho^2 \Delta \sin^2 \theta} \end{pmatrix}, \quad (5)$$

which satisfies  $g^{\mu\alpha}g_{\alpha\nu} = \delta_\nu^\mu$ .

Suppose a test particle with mass  $m$  and charge  $q$  is traveling within the background of a rotating charged black hole. The Lagrangian for this motion can be written as

$$\begin{aligned} \mathcal{L} &= \frac{1}{2}g_{\mu\nu}\frac{dx^\mu}{d\lambda}\frac{dx^\nu}{d\lambda} + eA_\mu\frac{dx^\mu}{d\lambda} \\ &= -\frac{1}{2}\frac{\Delta - a^2 \sin^2 \theta}{\rho^2}\dot{t}^2 - \frac{a \sin^2 \theta(2Mr - Q^2)}{\rho^2}\dot{t}\dot{\varphi} + \frac{1}{2}\frac{\rho^2}{\Delta}\dot{r}^2 + \frac{1}{2}\rho^2\dot{\theta}^2 \\ &\quad + \frac{1}{2}\frac{(r^2 + a^2)^2 - \Delta a^2 \sin^2 \theta}{\rho^2}\sin^2 \theta\dot{\varphi}^2 - \frac{eQr}{\rho^2}\dot{t} + \frac{eQra \sin^2 \theta}{\rho^2}\dot{\varphi}, \end{aligned} \quad (6)$$

where  $e = \frac{q}{m}$  is the charge-to-mass ratio,  $\lambda$  is the affine parameter and the dot denotes the differential with respect to  $\lambda$ . The canonical momenta  $p_\mu$  are defined by

$$p_t = -\frac{\partial \mathcal{L}}{\partial \dot{t}} = \frac{\Delta - a^2 \sin^2 \theta}{\rho^2}\dot{t} + \frac{2Mr - Q^2}{\rho^2}a \sin^2 \theta\dot{\varphi} + \frac{eQr}{\rho^2}, \quad (7)$$

$$p_r = \frac{\partial \mathcal{L}}{\partial \dot{r}} = \frac{\rho^2}{\Delta}\dot{r}, \quad (8)$$

$$p_\theta = \frac{\partial \mathcal{L}}{\partial \dot{\theta}} = \rho^2\dot{\theta}, \quad (9)$$

$$p_\varphi = \frac{\partial \mathcal{L}}{\partial \dot{\varphi}} = \frac{(r^2 + a^2)^2 - \Delta a^2 \sin^2 \theta}{\rho^2}\sin^2 \theta\dot{\varphi} - \frac{2Mr - Q^2}{\rho^2}a \sin^2 \theta\dot{t} + \frac{eQra \sin^2 \theta}{\rho^2}. \quad (10)$$

The Hamiltonian is obtained by the Legendre transformation

$$\mathcal{H} = -p_t\dot{t} + p_r\dot{r} + p_\theta\dot{\theta} + p_\varphi\dot{\varphi} - \mathcal{L} = \frac{1}{2}g_{\mu\nu}\frac{dx^\mu}{d\lambda}\frac{dx^\nu}{d\lambda}. \quad (11)$$

There existed four constants in this motion: the rest mass  $m$ , the energy  $E$ , the Carter constant  $D$  and the the angular momentum  $L_z$  in  $z$ -direction, which are defined by

$$m^2 = -2\mathcal{H} = -g_{\mu\nu}\frac{dx^\mu}{d\lambda}\frac{dx^\nu}{d\lambda}, \quad (12)$$

$$E = p_t = \frac{\Delta - a^2 \sin^2 \theta}{\rho^2}\dot{t} + \frac{2Mr - Q^2}{\rho^2}a \sin^2 \theta\dot{\varphi} + \frac{eQr}{\rho^2}, \quad (13)$$

$$L_z = p_\varphi = \frac{(r^2 + a^2)^2 - \Delta a^2 \sin^2 \theta}{\rho^2}\sin^2 \theta\dot{\varphi} - \frac{2Mr - Q^2}{\rho^2}a \sin^2 \theta\dot{t} + \frac{eQra \sin^2 \theta}{\rho^2}, \quad (14)$$

$$D = \rho^4\dot{\theta}^2 - \cos^2 \theta\left(a^2(E^2 - m^2) - \frac{L_z^2}{\sin^2 \theta}\right). \quad (15)$$

Within these constants, the equations of motion  $\dot{x}^\mu = \frac{\partial \mathcal{H}}{\partial p_\mu}, \dot{p}_\mu = -\frac{\partial \mathcal{H}}{\partial x^\mu}$  can be rewritten as the decoupled, first-order equations

$$\rho^2 \dot{t} = \frac{1}{\Delta} \left[ E((r^2 + a^2)^2 - \Delta a^2 \sin^2 \theta) + aL_z(Q^2 - 2Mr) - eQr(r^2 + a^2) \right], \quad (16)$$

$$\rho^2 \dot{\varphi} = \frac{1}{\Delta} \left[ aE(2Mr - Q^2) + \frac{L_z}{\sin^2 \theta} (\Delta - a^2 \sin^2 \theta) - aQer \right], \quad (17)$$

$$\rho^4 \dot{\theta}^2 \equiv \Theta = D + \cos^2 \theta (a^2(E^2 - m^2) - \frac{L_z^2}{\sin^2 \theta}), \quad (18)$$

$$\begin{aligned} \rho^4 \dot{r}^2 \equiv R = & (E^2 - m^2)r^4 + 2(m^2M - eQE)r^3 + [a^2(E^2 - m^2) + (e^2 - m^2)Q^2 - L_z^2 - D]r^2 \\ & + 2[M((L_z - aE)^2 + D) + aQe(L_z - aE)]r - Q^2[(L_z - aE)^2 + D] - a^2D, \end{aligned} \quad (19)$$

where we have introduced the variables  $R = \rho^4 \dot{r}^2$  and  $\Theta = \rho^4 \dot{\theta}^2$  for brevity.

Introducing Hamilton's principal function  $S$  via

$$g_{\mu\nu} \dot{x}^\nu + qA_\mu = \frac{\partial S}{\partial x^\mu} \equiv p_\mu, \quad (20)$$

leads to the corresponding Hamilton–Jacobi equation

$$-2 \frac{\partial S}{\partial \lambda} = g^{\mu\nu} \left( \frac{\partial S}{\partial x^\mu} - qA_\mu \right) \left( \frac{\partial S}{\partial x^\nu} - qA_\nu \right). \quad (21)$$

By demonstrating that the Hamilton–Jacobi equation (21) for test particles is separable, Carter [10] first established the existence of a fourth constant of geodesic motion in Kerr spacetime – now known as the Carter constant  $D$ . As a consequence of the separability, the abbreviated action  $S$  is constrained to a particular form

$$S = \frac{1}{2}m^2\lambda - Et + L_z\varphi + \int^r \frac{\sqrt{R}}{\Delta} dr + \int^\theta \sqrt{\Theta} d\theta. \quad (22)$$

Due to the constancy of  $D$ , general geodesic motion is no longer planar; thus, the orbits occur in the three-dimensional coordinate space  $(r, \theta, \varphi)$ . The equations of motion follow from the vanishing of the partial derivatives of the abbreviated action  $S$  with respect to the four constants  $D, E, m, L_z$ . Setting  $\frac{\partial S}{\partial D} = 0$ , one obtains the constraint condition satisfied in the  $(r, \theta)$  coordinates

$$\int^r \frac{dr}{\sqrt{R}} = \int^\theta \frac{d\theta}{\sqrt{\Theta}}. \quad (23)$$

Similarly, setting  $\frac{\partial S}{\partial m} = 0$ ,  $\frac{\partial S}{\partial E} = 0$  and  $\frac{\partial S}{\partial L_z} = 0$ , we find

$$\lambda = \int^r \frac{r^2}{\sqrt{R}} dr + a^2 \int^\theta \frac{\cos^2 \theta}{\sqrt{\Theta}} d\theta, \quad (24)$$

$$t = E\lambda + \int^r \left( (2ME - eQ)r^3 - EQ^2r^2 - a[2M(L_z - aE) + aeQ]r + aQ^2(L_z - aE) \right) \frac{dr}{\Delta\sqrt{R}}, \quad (25)$$

$$\varphi = a \int^r [(2ME - eQ)r - L_z a - EQ^2] \frac{dr}{\Delta\sqrt{R}} + L_z \int^\theta \csc^2 \theta \frac{d\theta}{\sqrt{\Theta}}. \quad (26)$$

The above simplifications have been effected with Eq.(23).

Consider test particles incident from infinity. A portion of these particles will fall into the black hole, while another portion will be scattered back to infinity. Between these two cases lies a critical scenario, where particles are neither captured by the black hole nor escape to infinity, but instead asymptotically approach a critical radius at a finite distance. Next, we will provide a detailed analysis of the critical orbital solutions for test particle motion—including both null and time-like orbits — in Schwarzschild, Reissner-Nordström, Kerr, and Kerr-Newman spacetimes.

### III. NEUTRAL PARTICLES TRAVELING IN A SCHWARZSCHILD SPACE-TIME

In this section, we consider the motion of neutral particles in a Schwarzschild black hole. In this case, parameters  $a = Q = e = 0$ . The equations (16) - (19) of motion reduce to

$$\dot{t} = \frac{r^2}{\Delta} E, \quad (27)$$

$$\dot{\varphi} = \frac{L_z}{r^2 \sin^2 \theta}, \quad (28)$$

$$\dot{\theta}^2 = \frac{1}{r^4} \left( L^2 - \frac{L_z^2}{\sin^2 \theta} \right), \quad (29)$$

$$r^4 \dot{r}^2 = (E^2 - m^2)r^4 + 2m^2 M r^3 - L^2 \Delta, \quad (30)$$

where  $L^2 = D + L_z^2$  is the angular momentum. In spherically symmetric spacetimes, the Carter constant  $D$  reduces to the constant angular momentum  $L^2$ , which can be further expressed as

$$L^2 = r^4 (\dot{\theta}^2 + \sin^2 \theta \dot{\varphi}^2) \equiv r^4 \frac{d\Omega^2}{d\lambda^2}, \quad (31)$$

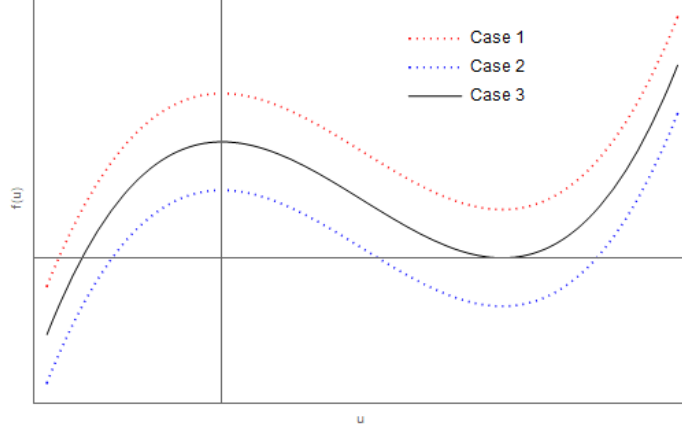


FIG. 1. All possible root configurations of  $f(u) = 0$ . In Case 1, where there are no real roots for  $u > 0$ , a photon incident from infinity will be absorbed by the black hole. In Case 2, characterized by two distinct real roots within  $u > 0$ , the photon will be scattered. Case 3 corresponds to the critical orbit, where a double root occurs at  $u_c > 0$ . In this critical case, as we will discuss later, the photon is neither absorbed nor scattered but instead approaches a circular orbit at a finite radius  $r_c = \frac{1}{u_c}$ .

where  $d\Omega^2 = d\theta^2 + \sin^2\theta d\varphi^2$ . When the square of the angular momentum  $L^2$  is constant, namely  $d\Omega^2 = \text{constant}$ , it implies that the geodesics in this spacetime are confined to a single plane. This conclusion also holds for other spherically symmetric spacetimes. To simplify calculations, we can restrict our discussion to orbital motion in the equatorial plane  $\theta = \frac{\pi}{2}$ . Orbits in other planes can be obtained by appropriately rotating the equatorial plane. In the equatorial case,  $\dot{\theta} = 0, L = L_z$ . We are not concerned with the solution for time  $t$ , and the orbital equations (28) - (30) further reduce to

$$\left(\frac{dr}{d\varphi}\right)^2 = \frac{E^2 - m^2}{L^2}r^4 + 2m^2\frac{M}{L^2}r^3 - r^2 + 2Mr. \quad (32)$$

Since the condition  $\left(\frac{dr}{d\varphi}\right)^2 \geq 0$  must hold, particles coming from infinity must have  $E \geq m$ . The case  $E = m$  merely represents particles falling freely from rest and is not considered a critical orbit. Therefore, we restrict our analysis to the case  $E > m$ . By defining  $u = 1/r$ , Eq. (32) can be reformulated as

$$\left(\frac{du}{d\varphi}\right)^2 = 2Mu^3 - u^2 + \frac{2m^2M}{L^2}u + \frac{E^2 - m^2}{L^2} \equiv f(u). \quad (33)$$

### A. null geodesic

In the case of a null geodesic  $m = 0$ , the function  $f(u)$  simplifies to

$$f(u) = 2Mu^3 - u^2 + \frac{E^2}{L^2}. \quad (34)$$

The orbital types are classified according to the roots of  $f(u) = 0$ . Since  $f(0) = \frac{E^2}{L^2} > 0$ , a negative root is always present. The three possible orbital types — absorption, scattering, and critical — correspond to the nature of the remaining roots, see Fig.1. For the critical orbit, the remaining two positive roots coincide at  $u_c$ , meaning:

$$f(u_c) = 0, \quad f'(u_c) = 0, \quad (35)$$

where prim denotes differentiation with respect to its variable. Solving these equations, one can obtain

$$u_c = \frac{1}{3M}, \quad \frac{E_c^2}{L_c^2} = \frac{1}{27M^2}. \quad (36)$$

The critical radius  $r_c = \frac{1}{u_c} = 3M$  defines the photon sphere, while the critical impact parameter  $R_c = \frac{L_c}{E_c} = 3\sqrt{3}M$  corresponds to the radius of the black hole's shadow as seen from infinity.

Inserting the critical impact parameter into (34), the orbital equation turns into

$$\left(\frac{du}{d\varphi}\right)^2 = 2M(u - u_c)^2\left(u + \frac{u_c}{2}\right), \quad (37)$$

where the negative root  $u_* = -\frac{u_c}{2}$ . The solution is given by

$$u = -\frac{1}{6M} + \frac{1}{2M} \tanh^2 \frac{1}{2}(\varphi - \varphi_0), \quad (38)$$

where  $\varphi_0$  is the constant of integration. The critical null geodesic is shown in Fig. 2, depicting the trajectory of a massless particle from infinity as it spirals inward, asymptotically winding around the circle at  $r_c = 3M$ .

### B. time-like geodesic

Unlike the case of null geodesics, the critical radius for timelike geodesics depends on the parameter  $E$  and  $L$ .<sup>1</sup> When  $E^2 > m^2$ , we have  $f(0) = \frac{E^2 - m^2}{L^2} > 0$ , implying the existence of

---

<sup>1</sup> When a triple root occurs, the critical radius can be uniquely determined as  $u_c = \frac{1}{6M}$ . However, this corresponds to the bound case where  $E^2 < m^2$ .

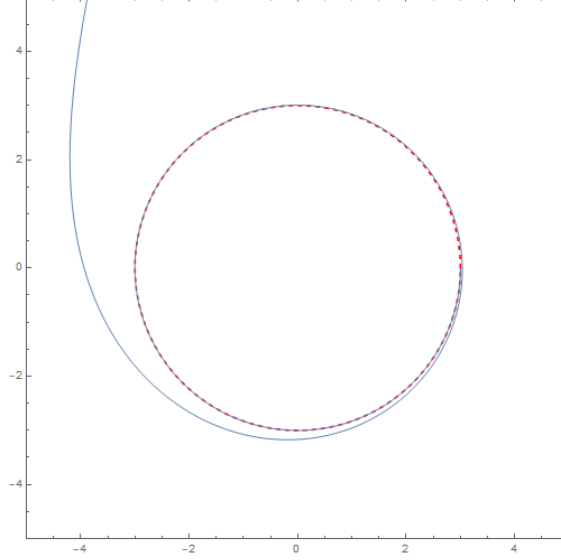


FIG. 2. The critical orbits for the null geodesic in the Schwarzschild metric. The mass is chosen to be  $M = 1$  and the constant  $\varphi_0 = 0$ . The dashed line is the location of the photon sphere.

one negative root. If the other two real roots coincide, the conditions (35) are also satisfied, namely

$$2Mu_c^3 - u_c^2 + \frac{2m^2M}{L^2}u_c + \frac{E^2 - m^2}{L^2} = 0, \quad (39)$$

$$3Mu_c^2 - u_c + \frac{m^2M}{L^2} = 0. \quad (40)$$

The solutions are given by

$$L_c^2 = \frac{m^2M}{u_c - 3Mu_c^2}, \quad (41)$$

$$E_c^2 - m^2 = \frac{(4Mu_c - 1)u_cm^2M}{1 - 3Mu_c}, \quad (42)$$

with the conditions  $L_c^2 > 0, E_c^2 - m^2 > 0$  requiring  $u_c \in (\frac{1}{4M}, \frac{1}{3M})$ . Substituting the critical impact parameter into equation (33), the orbital equation reduces to

$$\left(\frac{du}{d\varphi}\right)^2 = 2M(u - u_c)^2\left(u + 2u_c - \frac{1}{2M}\right), \quad (43)$$

where the negative root is  $u_* = \frac{1}{2M} - 2u_c$  and  $u_c$  lies in the interval  $(\frac{1}{4M}, \frac{1}{3M})$ . Mathematical analysis shows

$$u = u_c - \frac{1}{M} \frac{6Mu_c - 1}{1 + \cosh(\sqrt{6Mu_c - 1}(\varphi - \varphi_0))}. \quad (44)$$

The critical time-like geodesic in the Schwarzschild background is plotted in Fig.3.

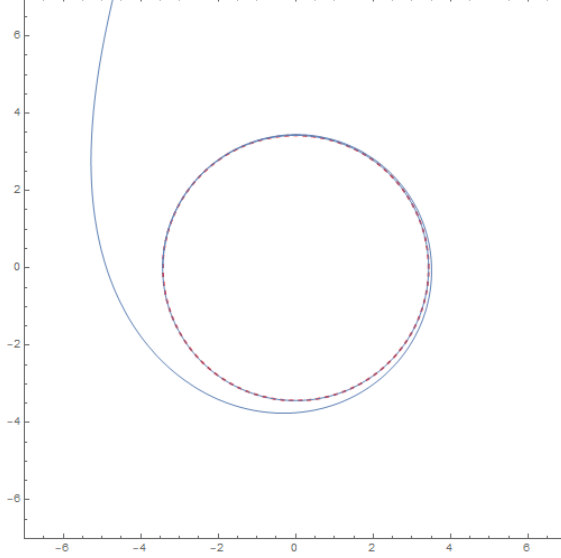


FIG. 3. The critical orbits for the time-like geodesic in the Schwarzschild metric. The parameters are chosen to be  $M = 1, \varphi_0 = 0, u_c = \frac{7}{24}$ . The dashed line is the location of the critical radius  $r_c = \frac{1}{u_c}$ .

#### IV. CHARGED PARTICLES TRAVELING IN A REISSNER-NORDSTRÖM SPACE-TIME

In this section, we study the motion of charged particles traveling in a Reissner-Nordström black hole  $a = 0$ . The equations (16) - (19) governing this motion are reduces to

$$\dot{t} = \frac{r}{\Delta}(Er - eQ), \quad (45)$$

$$\dot{\varphi} = \frac{L_z}{r^2 \sin^2 \theta}, \quad (46)$$

$$\dot{\theta}^2 = \frac{1}{r^4} \left( L^2 - \frac{L_z^2}{\sin^2 \theta} \right), \quad (47)$$

$$r^4 \dot{r}^2 = (E^2 - m^2)r^4 + 2(m^2 M - eQE)r^3 - L^2 \Delta. \quad (48)$$

Similar to geodesics in Schwarzschild spacetime, the square of the angular momentum  $L^2$  is constant. Thus, the world lines are confined to the same plane. Notice that a charged test particle in Reissner-Nordström spacetime will no longer follow geodesics. The orbital equations in the plane are also given by  $\left(\frac{du}{d\varphi}\right)^2 = f(u)$ , where

$$f(u) = -Q^2 u^4 + 2Mu^3 - \left(1 + \frac{m^2 - e^2}{L^2} Q^2\right) u^2 + 2 \frac{m^2 M - eQE}{L^2} u + \frac{E^2 - m^2}{L^2}. \quad (49)$$

Now  $f(u)$  becomes a quartic function in  $u$ . Given that  $f(0) > 0$ , the equation  $f(u) = 0$  must have one negative real root  $u_*^-$  and one positive real root  $u_*^+$ . Therefore, the zeros of the function  $f(u)$  may fall into the following cases: (i) there exist four real roots, three of which are coincident; (ii) there exist four real roots, two of which are coincident; (iii) there exist two real roots and two complex roots. This paper will primarily be concerned with cases (i) and (ii). They all satisfy  $f(u_c) = 0, f'(u_c) = 0$ .

### A. null geodesic

The null geodesic  $m = e = 0$  in the Reissner-Nordström geometry is governing by function

$$f(u) = -Q^2 u^4 + 2Mu^3 - u^2 + \frac{E^2}{L^2}. \quad (50)$$

In the critical case  $f(u_c) = 0, f'(u_c) = 0$ , it is easy to obtain

$$u_c = \frac{3M \pm \sqrt{9M^2 - 8Q^2}}{4Q^2}, \quad (51)$$

$$\frac{E_c^2}{L_c^2} = -\frac{27M^4 - 36M^2Q^2 + 8Q^4 \pm 9M^3\sqrt{9M^2 - 8Q^2} \mp 8MQ^2\sqrt{9M^2 - 8Q^2}}{32Q^6}. \quad (52)$$

For photons incident from infinity, they will initially encounter the larger critical radius  $r_c = \frac{1}{u_c}$ , which is the scenario we will focus on in the subsequent analysis.

As in the Schwarzschild case, the shadow radius of a Reissner-Nordström black hole, as seen by a distant observer, is given by  $R_c = \frac{L_c}{E_c}$ . For small values of the charge  $Q$ , a Taylor series expansion yields

$$u_c = \frac{1}{3M} \left( 1 + \frac{2Q^2}{9M^2} + O\left(\frac{Q^4}{M^4}\right) \right), \quad (53)$$

$$R_c = 3\sqrt{3}M \left( 1 - \frac{Q^2}{6M^2} + O\left(\frac{Q^4}{M^4}\right) \right). \quad (54)$$

Thus, compared to an uncharged black hole, a charged black hole possesses a smaller photon sphere and therefore casts a smaller shadow. In the extreme case  $Q = M$ , the smallest possible photon sphere and shadow radius are obtained

$$r_c^{\text{ex}} = \frac{1}{u_c^{\text{ex}}} = 2M, \quad R_c^{\text{ex}} = 4M. \quad (55)$$

Given the condition for the existence of the horizon  $Q < M$ , the case of three coincident real roots cannot occur. Thus, the function  $f(u)$  in the critical case can only degenerate to

$$f(u) = -Q^2(u - u_c)^2(u - u_*^-)(u - u_*^+), \quad (56)$$

where

$$u_*^\pm = \frac{M + \sqrt{9M^2 - 8Q^2} \pm 2\sqrt{M(M + \sqrt{9M^2 - 8Q^2})}}{4Q^2}, \quad (57)$$

and  $u_*^- < 0 < u_c < u_*^+$ . Solving the equation  $\frac{du}{d\varphi} = \sqrt{f(u)}$ , one obtains

$$u = u_c - \frac{2(u_*^- - u_c)(u_c - u_*^+)}{u_*^- + u_*^+ - 2u_c + (u_*^+ - u_*^-) \cosh\left(Q(\varphi - \varphi_0)\sqrt{(u_c - u_*^-)(u_*^+ - u_c)}\right)}. \quad (58)$$

The plot of this solution resembles Fig.2 and is omitted here.

## B. time-like world line

The conditions for time-like critical orbits are

$$-Q^2u^4 + 2Mu^3 - \left(1 + \frac{m^2 - e^2}{L^2}Q^2\right)u^2 + 2\frac{m^2M - eQE}{L^2}u + \frac{E^2 - m^2}{L^2} = 0, \quad (59)$$

$$-2Q^2u^3 + 3Mu^2 - \left(1 + \frac{m^2 - e^2}{L^2}Q^2\right)u + \frac{m^2M - eQE}{L^2} = 0. \quad (60)$$

Assume that the critical orbits have radius  $r_c = \frac{1}{u_c}$ , it follows that the energy  $E$  and the angular momentum are given by

$$E_c = \frac{1}{2Y_c} \left( \Delta_c \sqrt{4m^2Y_c + e^2Q^2u_c^2} + eQu_cP_c \right), \quad (61)$$

$$L_c^2 = \frac{1}{2u_cY_c^2} \left( 2m^2(M - Q^2u_c)Y_c - eQ\Delta_c(\sqrt{4m^2Y_c + e^2Q^2u_c^2} - eQu_c) \right), \quad (62)$$

where

$$\Delta_c = 1 - 2Mu_c + Q^2u_c^2, \quad (63)$$

$$Y_c = 1 - 3Mu_c + 2Q^2u_c^2, \quad (64)$$

$$P_c = 1 - 4Mu_c + 3Q^2u_c^2. \quad (65)$$

These equations require  $4m^2Y_c + e^2Q^2u_c^2 > 0$ , namely  $u_c^- < u_c < u_c^+$  where

$$u_c^\pm = \frac{2\left(3m^2M \pm \sqrt{-e^2m^2Q^2 + 9m^4M^2 - 8m^4Q^2}\right)}{e^2Q^2 + 8m^2Q^2}. \quad (66)$$

A fundamentally new scenario arises—the case of triply coincident roots. For this situation to occur, the additional constraint  $f''(u) = 0$  must be satisfied, namely

$$6Q^2u^2 - 6Mu + 1 + \frac{m^2 - e^2}{L^2}Q^2 = 0. \quad (67)$$

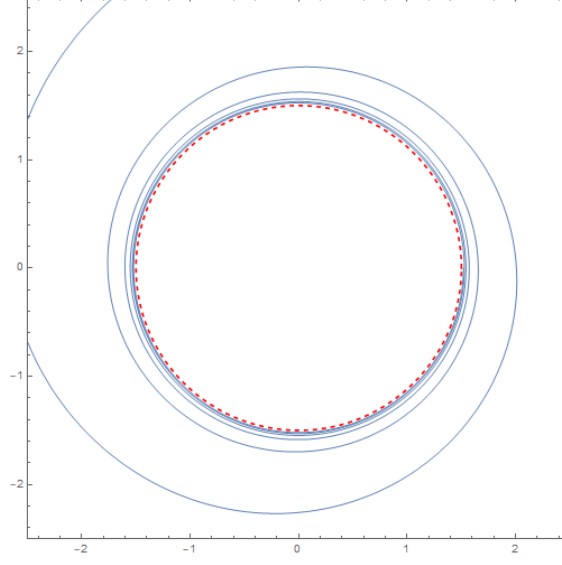


FIG. 4. The critical orbits of case (i) for the time-like world line in the Reissner–Nordström metric. The parameters are chosen to be  $u_c = \frac{2}{3M}$ ,  $e = 1.5m$ ,  $Q = \frac{3mM}{\sqrt{e^2+8m^2}}$ ,  $M = 1$ ,  $\varphi_0 = 0$ . The dashed line is the location of the critical radius  $r_c = \frac{1}{u_c}$ .

Eliminating  $L^2$  with the aid of Eq. (62), one obtains

$$(6Q^2u_c^2 - 6Mu_c + 1)[2m^2(M - Q^2u_c)Y_c - eQ\Delta_c(\sqrt{4m^2Y_c + e^2Q^2u_c^2} - eQu_c)] + 2(m^2 - e^2)Q^2u_cY_c^2 = 0. \quad (68)$$

Note that while the above equation may admit multiple solutions, only those satisfying the condition of  $u_c^- < u_c < u_c^+$  being a triple root are valid. In particular, when  $e = 0$ , the above equation reduces to

$$4Q^4u_c^3 - 9MQ^2u_c^2 + 6M^2u_c - M = 0. \quad (69)$$

This equation determined the minimal radius for a stable circular orbit in Reissner–Nordström geometry. In the critical case (i), the planar orbital equation takes the form

$$\left(\frac{du}{d\varphi}\right)^2 = -Q^2(u - u_c)^3\left(u - \frac{2M - 3Q^2u_c}{Q^2}\right), \quad (70)$$

where the negative root  $u_*^- = \frac{2M - 3Q^2u_c}{Q^2}$  shows that the triple root satisfies  $u_c > \frac{2M}{3Q^2}$ . The solution is

$$u = u_c + \frac{2(M - 2Q^2u_c)}{Q^2 + (M - 2Q^2u_c)^2(\varphi - \varphi_0)^2}, \quad (71)$$

and one example of this orbit is plotted in Fig.4.

In the critical case (ii), the planar orbital equation takes the form

$$\left(\frac{du}{d\varphi}\right)^2 = -Q^2(u - u_c)^2(u - u_*^-)(u - u_*^+), \quad (72)$$

where

$$u_*^\pm = \frac{L_c^2(M - Q^2u_c) \pm |L_c|\sqrt{Q^4(m^2 - e^2 - 2L_c^2u_c^2) + L_c^2Q^2(2Mu_c + 1) + L_c^2M^2}}{L_c^2Q^2}, \quad (73)$$

and  $L_c^2$  is expressed in Eq. (62). This equation shares the same form as the null geodesic orbital equation (56), hence its solution can be expressed as Equation (58), albeit with different parameters  $u_c$  and  $u_*^\pm$ .

## V. NEUTRAL PARTICLES TRAVELING IN A KERR SPACE-TIME

In this section, we study critical orbits of neutral particles traveling in the Kerr geometry.

In the case of  $Q = e = 0$ , the equations (16) - (19) reduce to

$$\rho^2\dot{t} = \frac{1}{\Delta} [E((r^2 + a^2)^2 - \Delta a^2 \sin^2 \theta) - 2ML_z ar], \quad (74)$$

$$\rho^2\dot{\varphi} = \frac{1}{\Delta} \left[ 2MaEr + \frac{L_z}{\sin^2 \theta} (\Delta - a^2 \sin^2 \theta) \right], \quad (75)$$

$$\rho^4\dot{\theta}^2 \equiv \Theta = D + \cos^2 \theta (a^2(E^2 - m^2) - \frac{L_z^2}{\sin^2 \theta}), \quad (76)$$

$$\begin{aligned} \rho^4\dot{r}^2 \equiv R &= (E^2 - m^2)r^4 + 2m^2Mr^3 + [a^2(E^2 - m^2) - L_z^2 - D]r^2 \\ &+ 2M((L_z - aE)^2 + D)r - a^2D, \end{aligned} \quad (77)$$

where Eq. (19) reduces to Eq. (77).

In the following discussion, we introduce new variables

$$\xi = \frac{L_z}{\sqrt{E^2 - m^2}}, \quad \eta = \frac{D}{E^2 - m^2}, \quad \chi^2 = \frac{E^2}{E^2 - m^2}. \quad (78)$$

Then, functions  $R$  and  $\Theta$  can be rewritten as

$$\frac{R}{E^2 - m^2} = r^4 + 2M(\chi^2 - 1)r^3 + (a^2 - \xi^2 - \eta)r^2 + 2M[\eta + (\xi - a\chi)^2]r - a^2\eta, \quad (79)$$

$$\frac{\Theta}{E^2 - m^2} = \eta + a^2 \cos^2 \theta - \xi^2 \cot^2 \theta. \quad (80)$$

We begin by considering the solution in the  $\theta$  direction, before discussing the  $r$ -motion. The  $\theta$ -motion is governed by the integral of  $\int \frac{d\theta}{\sqrt{\Theta}}$ . For this integral to be real-valued, the

condition  $\eta + (a - \xi)^2 \geq 0$  must be satisfied. Let's define  $\cos \theta = \mu$  as the variable of integration, then  $\int \frac{d\theta}{\sqrt{\tilde{\Theta}}} = -\int \frac{d\mu}{\sqrt{\tilde{\Theta}}}$  where

$$\frac{\tilde{\Theta}}{E^2 - m^2} = \eta - (\xi^2 + \eta - a^2)\mu^2 - a^2\mu^4. \quad (81)$$

The behavior of the  $\theta$ -motion is categorized by the cases  $\eta > 0, \eta < 0$  and  $\eta = 0$ .

1.  $\eta > 0$ : We can reexpress  $\tilde{\Theta}$  as

$$\frac{\tilde{\Theta}}{E^2 - m^2} = a^2(\mu_1^2 + \mu^2)(\mu_2^2 - \mu^2), \quad (82)$$

where

$$\mu_1^2 = \frac{1}{2a^2} \left( \sqrt{(\xi^2 + \eta - a^2)^2 + 4a^2\eta_c} + (\xi^2 + \eta - a^2) \right), \quad (83)$$

$$\mu_2^2 = \frac{1}{2a^2} \left( \sqrt{(\xi^2 + \eta - a^2)^2 + 4a^2\eta} - (\xi^2 + \eta - a^2) \right). \quad (84)$$

The requirement  $\tilde{\Theta} \geq 0$  implies  $0 \leq \mu^2 \leq \mu_2^2$ . Here,  $\mu^2 = 0$  corresponds to equatorial plane  $\theta = \frac{\pi}{2}$ . When  $\mu^2 = \mu_2^2$ , the orbits reach the turning angles  $\theta = \frac{\pi}{2} \pm \theta_m$ , where  $\theta_m = \arccos \mu_2$ . In other words, these orbits cross the equatorial plane and oscillate symmetrically about it. The integration yields

$$\frac{1}{\sqrt{E^2 - m^2}} \int^\mu \frac{d\mu}{\sqrt{\tilde{\Theta}}} = \frac{1}{a\sqrt{\mu_1^2 + \mu_2^2}} \text{EllipticF} \left[ \arcsin \frac{\sqrt{\mu_2^2 - \mu^2}}{\mu_2}, \frac{\mu_2^2}{\mu_1^2 + \mu_2^2} \right] + C, \quad (85)$$

where  $\text{EllipticF}[\phi, m]$  denotes the incomplete elliptic integral of the first kind and  $C$  is constant.

2.  $\eta = 0$ : In this special case, one obtains

$$\frac{\tilde{\Theta}}{E^2 - m^2} = a^2\mu^2(\mu_m^2 - \mu^2), \quad (86)$$

where  $\mu_m^2 = 1 - \frac{\xi^2}{a^2}$  and  $0 \leq \mu^2 \leq \mu_m^2 \leq 1$ . The integration yields

$$\frac{1}{\sqrt{E^2 - m^2}} \int^\mu \frac{d\mu}{\sqrt{\tilde{\Theta}}} = -\frac{1}{a\mu_m} \text{arctanh} \sqrt{1 - \frac{\mu^2}{\mu_m^2}} + C. \quad (87)$$

3.  $\eta < 0$ : Function  $\tilde{\Theta}$  can be reexpressed as

$$\frac{\tilde{\Theta}}{E^2 - m^2} = a^2(\mu_2^2 - \mu^2)(\mu^2 - \mu_1^2), \quad (88)$$

where

$$\mu_{1,2} = \frac{1}{2a^2} \left( (|\eta| + a^2 - \xi^2) \pm \sqrt{(|\eta| + a^2 - \xi^2)^2 - 4a^2|\eta|} \right). \quad (89)$$

Thus, the parameter  $\mu^2$  is restricted to  $0 \leq \mu_1^2 \leq \mu^2 \leq \mu_2^2 \leq 1$ . The conditions for  $\eta < 0$  are highly stringent  $|\eta| < a^2$  and  $0 < |\xi| \leq |a|$ . In such cases, the test particle will naturally enter the region of negative  $r$ , and its world line will end within this negative  $r$  region. However, to date, our analysis has not yielded a feasible set of physical parameters that would realize it. Here, we list it merely as a mathematical possibility for the sake of completeness. The integration yields

$$\frac{1}{\sqrt{E^2 - m^2}} \int^\mu \frac{d\mu}{\sqrt{\Theta}} = \frac{1}{a\mu_2} \text{EllipticF} \left[ \arcsin \sqrt{\frac{\mu_2^2(\mu^2 - \mu_1^2)}{\mu^2(\mu_2^2 - \mu_1^2)}}, \frac{\mu_2^2 - \mu_1^2}{\mu_2^2} \right] + C. \quad (90)$$

### A. null geodesic

We then consider the radial motion. For the massless particles traveling in Kerr geometry  $m = 0$  and  $\chi = 1$ ,  $R$  reduce to

$$\frac{R}{E^2} = r^4 + (a^2 - \xi^2 - \eta)r^2 + 2M[\eta + (\xi - a)^2]r - a^2\eta. \quad (91)$$

For the critical orbits  $R = 0$  and  $R' = 0$ , there are

$$r^4 + (a^2 - \xi^2 - \eta)r^2 + 2M[\eta + (\xi - a)^2]r - a^2\eta = 0, \quad (92)$$

$$4r^3 + 2(a^2 - \xi^2 - \eta)r + 2M[\eta + (\xi - a)^2] = 0. \quad (93)$$

The above equations yield two distinct pairs of solutions for  $\xi$  and  $\eta$ : one is

$$\xi_c = \frac{a^2 + r_c^2}{a}, \quad \eta_c = -\frac{r_c^4}{a^2}; \quad (94)$$

and the other is

$$\xi_c = \frac{r_c^2(r_c - 3M) + a^2(M + r_c)}{a(M - r_c)}, \quad \eta_c = \frac{r_c^3(4a^2M - (r_c - 3M)^2r_c)}{(r_c - M)^2a^2}. \quad (95)$$

Substituting solution (94) into equation (80), we find  $\Theta = -\frac{\rho^2 E^2}{a^2 \sin^2 \theta} \leq 0$ . Since physical motion requires  $\Theta \geq 0$ , this condition can only be satisfied if  $\theta = \theta_0$  remains constant which stands for the shear-free null-congruences. Our primary interest lies in the second set of solutions (95).

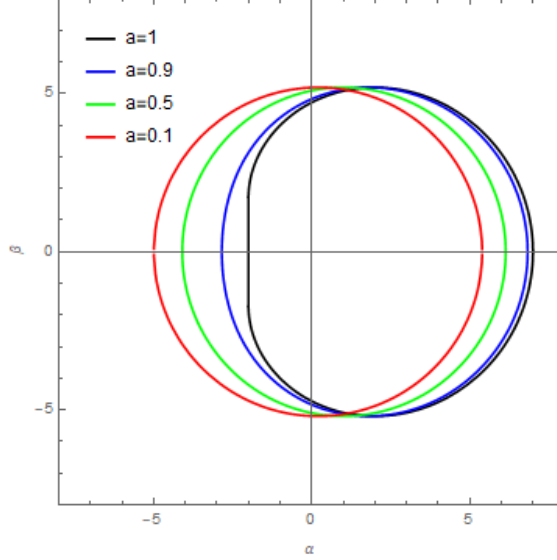


FIG. 5. The shadow of the Kerr black hole as seen by a distant observer in the equatorial plane. The Mass of the black hole is chosen to be  $M = 1$ .

The celestial coordinates are introduced by [22]

$$\alpha = \lim_{r_0 \rightarrow \infty} \left( -r_0^2 \sin \theta_0 \frac{d\varphi}{dr} \right) = -\xi \csc \theta_0, \quad (96)$$

$$\beta = \lim_{r_0 \rightarrow \infty} \left( r_0^2 \frac{d\theta}{dr} \right) = \pm(\eta + a^2 \cos^2 \theta_0 - \xi^2 \cot^2 \theta_0)^{1/2}, \quad (97)$$

where  $r_0$  is the distance from the black hole to the observer, and  $\theta_0$  is the viewing angle of the observer. If the observer lies in the equatorial plane  $\theta_0 = \frac{\pi}{2}$ , the celestial coordinates can be simply written as  $\alpha = -\xi, \beta = \pm\sqrt{\eta}$ . The apparent shape of the black hole is determined by the critical coordinates  $(\alpha_c, \beta_c)$ . Figure 5 depicts the shadow of the Kerr black hole as viewed from the equatorial plane.

There are two types of critical orbits, defined by the root structures of  $R = 0$ : (i) triple coincident roots and (ii) double coincident roots. In addition to Eqs. (92) and (93), the case of triple coincident roots requires that the condition  $R'' = 0$  also be satisfied, i. e.

$$6r^2 + a^2 - \xi^2 - \eta = 0. \quad (98)$$

Define  $\mu_0^2 = \frac{Mr_c}{3M^2 - 3Mr_c + r_c^2}$ , one can obtain the solution

$$\xi_c^* = \frac{3M^2 - r_c^2}{M} \mu_0, \quad \eta_c^* = 3r_c^2 \mu_0^2, \quad a_c^* = \frac{r_c}{\mu_0}. \quad (99)$$

Rewriting relation (99) yields

$$\frac{a_c^*}{M} = \sqrt{\frac{r_c}{M}} \sqrt{3 - 3\frac{r_c}{M} + \left(\frac{r_c}{M}\right)^2}. \quad (100)$$

This expression reveals a monotonic dependence:  $a_c^*$  increases with  $r_c$ . Given the constraints that the horizon exists  $0 \leq a \leq M$  and that the photon sphere lies outside the horizon  $r_+ \leq r_c$ , it follows that the case of triple coincident roots occurs only when  $a_c^* = M$  and  $r_c = r_+ = M$ , which shows  $\mu_0^2 = 1$  and  $\xi_c = 2M, \eta_c = 3M^2$ . Inserting the solutions into  $R$  and  $\tilde{\Theta}$ , one obtains

$$\frac{R}{E^2} = (r - M)^3(r + 3M), \quad (101)$$

$$\frac{\tilde{\Theta}}{E^2} = M^2(2\sqrt{3} + 3 + \mu^2)(2\sqrt{3} - 3 - \mu^2). \quad (102)$$

Mathematically, we obtain

$$\int \frac{dr}{E\sqrt{R}} = -\frac{\sqrt{(r - M)^3(r + 3M)}}{2M(r - M)^2} + C_1, \quad (103)$$

$$\int \frac{d\mu}{E\sqrt{\tilde{\Theta}}} = \frac{1}{M\sqrt{2\sqrt{3} + 3}} \text{EllipticF} \left[ \arcsin \frac{\mu}{\sqrt{2\sqrt{3} - 3}}, -\frac{2\sqrt{3} - 3}{2\sqrt{3} + 3} \right] + C_2, \quad (104)$$

where  $C_1, C_2$  are integration constants. Since  $\eta = 3M^2 > 0$ , the  $\theta$ -motion oscillates between  $(\frac{\pi}{2} - \theta_m, \frac{\pi}{2} + \theta_m)$ , where  $\theta_m = \arccos \mu_m$ . The actual constraint  $(r, \theta)$  given in (23) can now be integrated to yield

$$\int_{r_i}^r \frac{dr}{\sqrt{R}} = \left( \int_{\mu_i}^{\mu_m^1} - \int_{\mu_m^1}^{\mu_m^2} \dots + (-1)^{n-1} \int_{\mu_m^n}^{\mu} \right) \frac{d\mu}{\sqrt{\tilde{\Theta}}}, \quad (105)$$

where  $r_i, \mu_i$  are the initial conditions. Here, the limits  $\mu_m^n$  alternate between  $\mu_m$  and  $-\mu_m$ , specifically with  $\mu_m^{2k+1} = \pm\mu_m$  and  $\mu_m^{2k} = \mp\mu_m$ . The number of integrals  $n$  on the right-hand side equals the number of oscillations, which in turn depends on the final radial coordinate  $r$ . The solution of  $\varphi$  can be written as

$$\varphi = \frac{(r - 3M)}{6} \sqrt{\frac{r + 3M}{(r - M)^3}} - \frac{2}{\sqrt{2\sqrt{3} + 3}} \text{ElliptiPi} \left[ 2\sqrt{3} - 3, \arcsin \frac{\mu}{\sqrt{2\sqrt{3} - 3}}, -\frac{2\sqrt{3} - 3}{2\sqrt{3} + 3} \right] + C, \quad (106)$$

where  $\text{ElliptiPi}[n, \varphi, m]$  is the third elliptic integral. The numerical solution is shown in Fig.6.

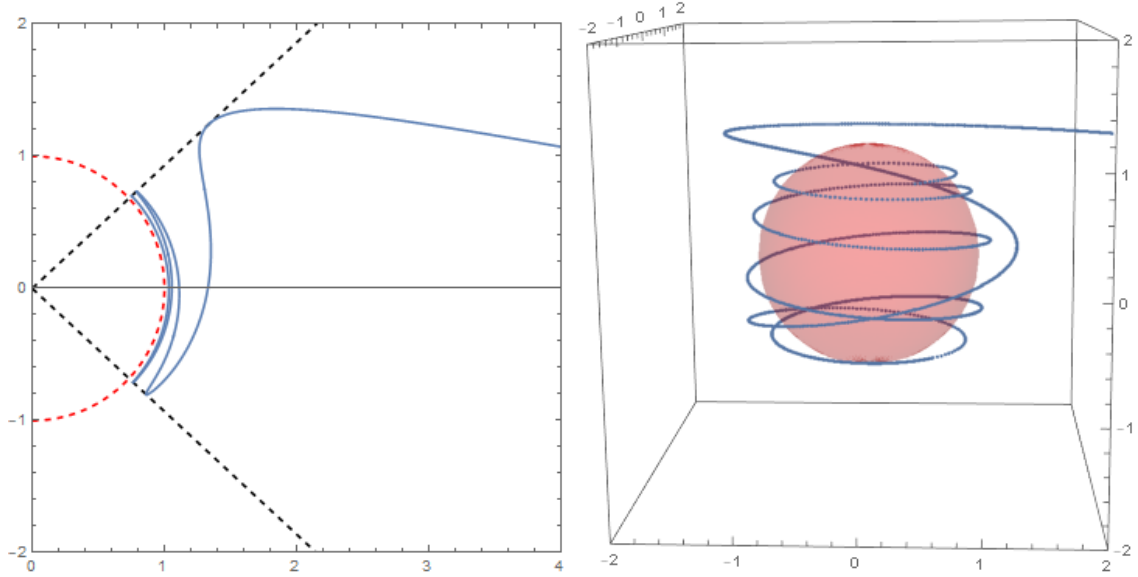


FIG. 6. The critical null orbits of triple coincident roots in Kerr spacetime. The left diagram illustrates the trajectory of null geodesic in the  $(r, \theta)$  plane, the right diagram shows the trajectory in three-dimensional space. The Mass of the black hole is chosen to be  $M = 1$  and the initial conditions are chosen to be  $r_i = 10, \mu_i = 0, \varphi_i = 0$ . The red dashed line (ball) is the photon sphere and the black dashed line is  $\mu = \pm\mu_m$ .

The critical null geodesics with double coincident roots can be analyzed similarly. Inserting  $\xi = \xi_c, \eta = \eta_c$  into Eqs. (91), we can reexpress  $R$  as

$$\frac{R}{E^2} = (r - r_c)^2 \left( r^2 + 2r_c r - \frac{a^2 \eta_c}{r_c^2} \right). \quad (107)$$

Define  $x = \frac{1}{r - r_c}$ , we obtains

$$\int^r \frac{dr}{E\sqrt{R}} = \frac{1}{\sqrt{c}} \ln[\sqrt{c}\sqrt{cx^2 + 4r_c x + 1} + cx + 2r_c] + C, \quad (108)$$

where  $c = 3r_c^2 - \frac{a^2 \eta_c}{r_c^2}$ . The interdependence of the coordinates  $r$  and  $\theta$  is specified in Eq. (23), while a detailed analysis of the  $\theta$  motion is provided in the previous subsection. The solution for  $\varphi$  is obtained via numerical integration. Critical null geodesics with double coincident roots are shown in Fig. 7.

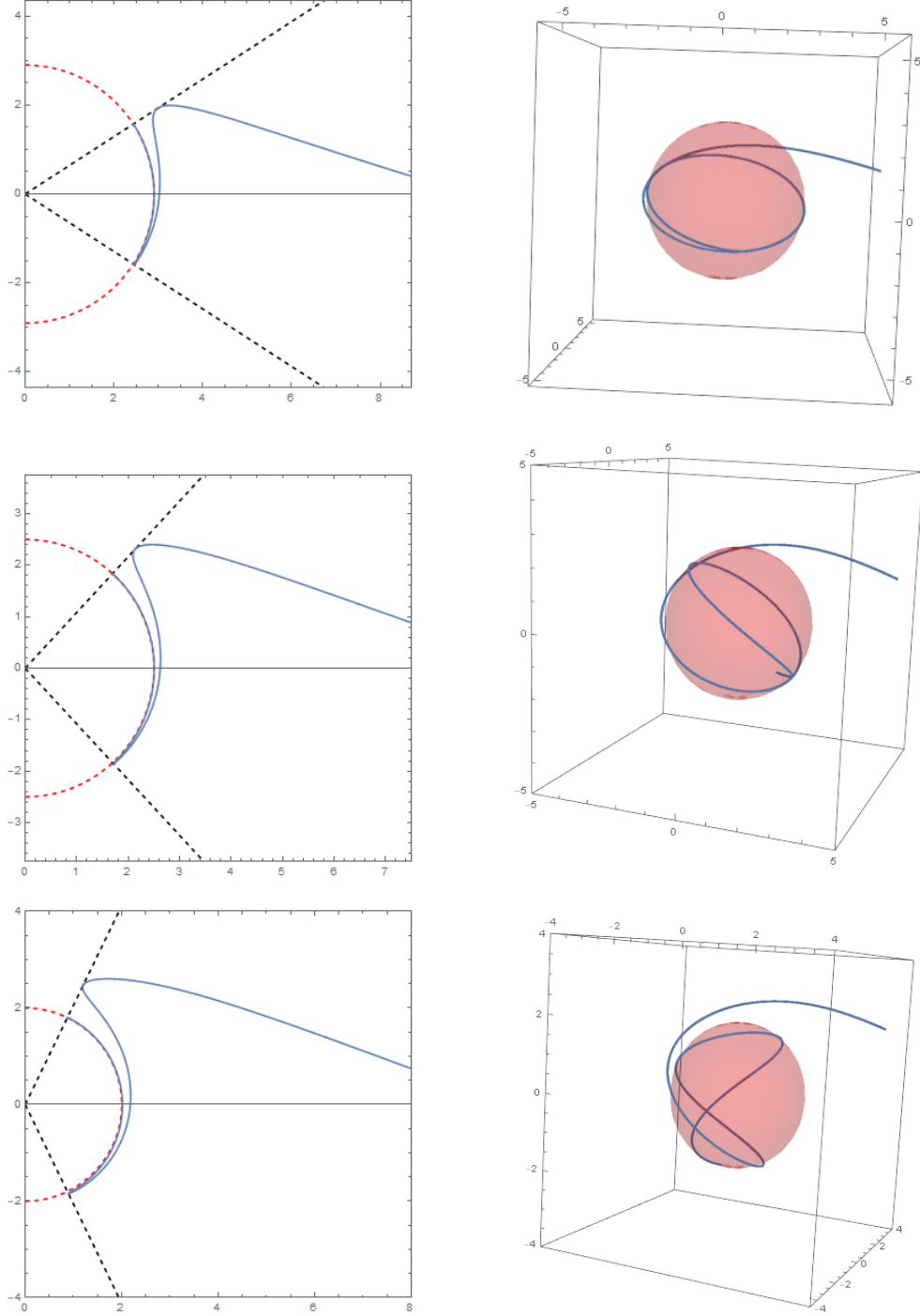


FIG. 7. The critical null orbits of double coincident roots in Kerr spacetime. The left diagram illustrates the trajectory of null geodesic in the  $(r, \theta)$  plane, while the right diagram shows the trajectory of null geodesic in three-dimensional space. The Mass of the black hole is chosen to be  $M = 1$  and the initial conditions are chosen to be  $r_i = 10, \mu_i = 0, \varphi_i = 0$ . The parameters for each row of images, from top to bottom, are  $a = 0.1, r_c = 2.9; a = 0.5, r_c = 2.5; a = 0.9, r_c = 2.0$ . The red dashed line (ball) is located at  $r = r_c$  and the black dashed line is  $\mu = \pm \mu_m$ .

## B. Timelike geodesic

For the timelike geodesics  $m \neq 0$ , we show that no triple root case exists when  $r_c > r_+$  in Appendix A. The condition for double roots,  $R = 0$  and  $R' = 0$ , yields

$$\eta_c = -\xi_c^2 - \frac{2aM\chi}{r_c - M}\xi_c - \frac{a^2M\chi^2 + a^2r_c + 3Mr_c^2\chi^2 - 3Mr_c^2 + 2r_c^3}{r_c - M}, \quad (109)$$

$$\xi_c = \frac{aM(r^2 - a^2)\chi \pm \sqrt{a^2M^2(r_c^2 - a^2)^2\chi^2 + 4K(r_c - M)a^2}}{a^2(r_c - M)}, \quad (110)$$

$$K = r_c\Delta^2(r_c) + M\chi^2(r_c^4 - 4Mr_c^3 + 2a^2r_c^2 + a^4). \quad (111)$$

The functions  $R$  can then be expressed as

$$\frac{R}{E^2 - m^2} = (r - r_c)^2 \left( r^2 + 2(r_c + M(\chi^2 - 1))r - \frac{a^2\eta_c}{r_c^2} \right). \quad (112)$$

Defining  $x = \frac{1}{r - r_c}$ , one can calculate the integrations to obtain

$$\int^r \frac{dr}{\sqrt{E^2 - m^2}\sqrt{R}} = \frac{1}{\sqrt{c}} \ln[\sqrt{c}\sqrt{cx^2 + 2bx + 1} + cx + b] + C, \quad (113)$$

where

$$b = 2r_c + M(1 - \chi^2), \quad (114)$$

$$c = 3r_c^2 + 2Mr_c(\chi^2 - 1) - \frac{a^2\eta_c}{r_c^2}. \quad (115)$$

The numerical results are plotted in Fig.8.

## VI. CHARGED PARTICLES TRAVELING IN A KERR-NEWMAN SPACE-TIME

In this section, we study the critical orbit of charged particles traveling in a Kerr-Newman background. We define

$$\xi = \frac{L_z}{\sqrt{E^2 - m^2}}, \quad \eta = \frac{D}{E^2 - m^2}, \quad \chi^2 = \frac{E^2}{E^2 - m^2}, \quad \tilde{e} = \frac{e}{\sqrt{E^2 - m^2}}, \quad (116)$$

and rewritten  $R$  as

$$\begin{aligned} \frac{R}{E^2 - m^2} = & r^4 + 2(M(\chi^2 - 1) - Q\chi)r^3 + (a^2 - \eta - \xi^2 + Q^2(\tilde{e}^2 - \chi^2 + 1))r^2 \\ & + 2(a\tilde{e}Q(\xi - a\chi) + M((\xi - a\chi)^2 + \eta))r + Q^2(2a\xi\chi - a^2\chi^2 - \eta - \xi^2) - a^2\eta. \end{aligned} \quad (117)$$

The integration of  $\int \frac{d\theta}{\sqrt{\Theta}}$  has been addressed in detail in the preceding section; here we concentrate solely on solving for  $r$ .

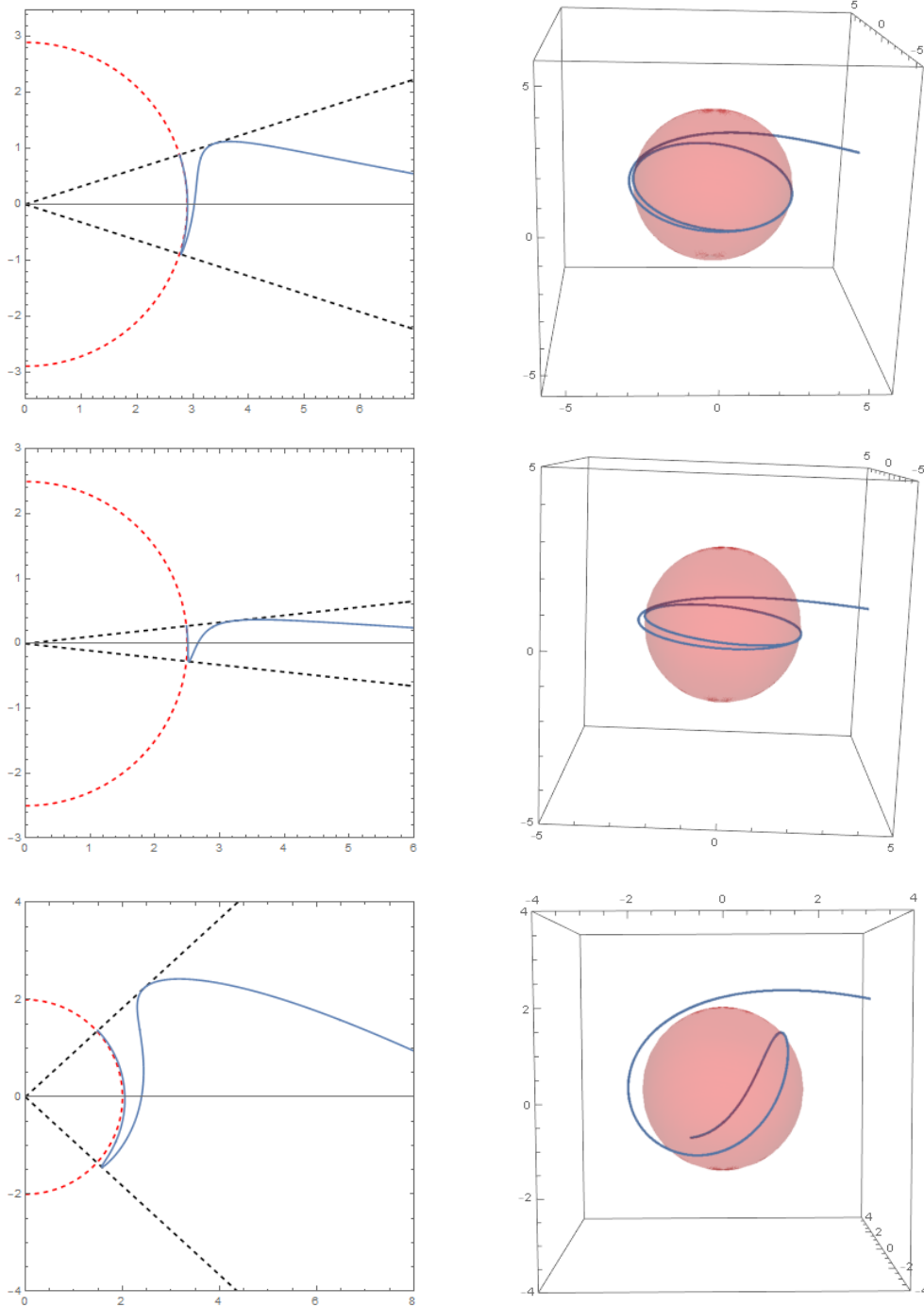


FIG. 8. The critical timelike geodesics in Kerr spacetime. The left diagram illustrates the trajectory of a timelike geodesic in the  $(r, \theta)$  plane, while the right diagram shows the trajectory in three-dimensional space. The Mass of the black hole is chosen to be  $M = 1$  and the initial conditions are chosen to be  $r_i = 10, \mu_i = 0, \varphi_i = 0$ . The parameters for each row of images, from top to bottom, are  $a = 0.1, r_c = 2.9, \chi = 1.02$ ;  $a = 0.5, r_c = 2.5, \chi = 1.4$ ;  $a = 0.9, r_c = 2.0, \chi = 4$ . The red dashed line (ball) is located at  $r = r_c$  and the black dashed line is  $\mu = \pm\mu_m$ .

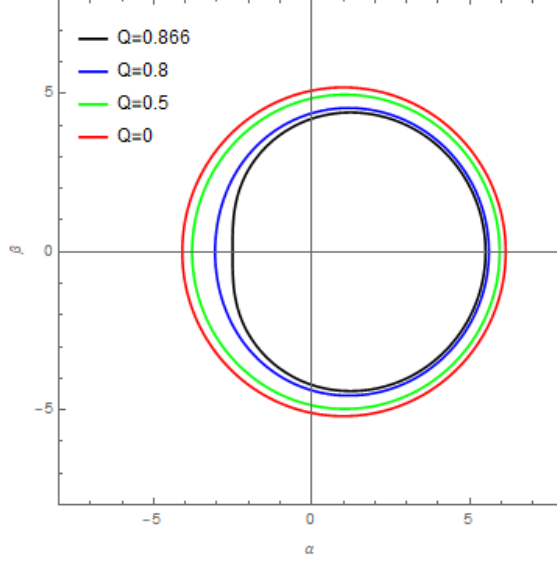


FIG. 9. The shadow of the KerrNewman black hole as seen by a distant observer in the equatorial plane. The Mass of the black hole is chosen to be  $M = 1$  and the parameter  $a = 0.5$ .

### A. null geodesic

In the case of null geodesics  $\tilde{e} = m = 0$  and  $\chi = 1$ , the function  $R$  would be further reduce to

$$\frac{R}{E^2} = r^4 + (a^2 - \xi^2 - \eta)r^3 + 2M[\eta + (\xi - a)^2]r - a^2\eta + Q^2(2a\xi - a^2 - \eta - \xi^2). \quad (118)$$

Solving  $R = 0$  and  $R' = 0$ , we obtains

$$\xi_c = \frac{a^2(M + r_c) + r_c(r_c(r_c - 3M) + 2Q^2)}{a(M - r_c)}, \quad (119)$$

$$\eta_c = -\frac{r_c^2 \left( 4a^2(Q^2 - Mr_c) + (r_c(r_c - 3M) + 2Q^2)^2 \right)}{a^2(M - r_c)^2}. \quad (120)$$

Similar to the previous section, we can compute the black hole shadow as seen by an observer in the equatorial plane. The figure 9 illustrates the influence of the new parameter  $Q$  on the black hole shadow.

For the critical orbits with triple coincident roots  $R = 0, R' = 0, R'' = 0$ , we obtain

$$\eta_c^* = \frac{r_c^3 (3Mr_c - 4Q^2)}{3M^2r_c - M(Q^2 + 3r_c^2) + r_c^3}, \quad (121)$$

$$\xi_c^* = \frac{3M^2r_c - MQ^2 - r_c^3}{\sqrt{M}\sqrt{3M^2r_c - M(Q^2 + 3r_c^2) + r_c^3}}, \quad (122)$$

$$\frac{a_c^*}{M} = \sqrt{\frac{r_c^3}{M^3} - 3\frac{r_c^2}{M^2} + 3\frac{r_c}{M} - \frac{Q^2}{M^2}}. \quad (123)$$

One can reexpress  $r_c = M - (M(M^2 - a^2 - Q^2))^{1/3}$ . Since the photon sphere lies outside the event horizon,  $r_+ \leq r_c$ , we have  $r_c = r_+ = M$ . It follows that  $\xi_c^* = \frac{M^2(3M^2 - 4Q^2)}{M^2 - Q^2}$ ,  $\eta_c^* = \frac{2M^2 - Q^2}{\sqrt{M^2 - Q^2}}$ ,  $a_c^* = \sqrt{M^2 - Q^2}$ . Then,  $\frac{R}{E^2}$  reduces to expression (102) and

$$\frac{\tilde{\Theta}}{E^2} = (M^2 - Q^2)(\mu_1^2 + \mu^2)(\mu_2^2 - \mu^2), \quad (124)$$

where  $\mu_{1,2}^2 = \frac{2M\sqrt{3M^2 - Q^2} \pm 3M^2}{M^2 - Q^2}$ . Therefore, the charge  $Q$  influences the geodesic by altering  $\theta_m$ . The integration of  $\int \frac{dr}{\sqrt{R}}$  is expressed as Eq. (103) and  $\int \frac{d\mu}{\sqrt{\tilde{\Theta}}}$  is expressed as Eq. (85) in the case of  $m = 0$ . The numerical results corresponding to this case are depicted in Fig. 10.

In the case of double coincident roots, one inserts  $\xi = \xi_c, \eta = \eta_c$  into Eq. (118) and obtains

$$\frac{R}{E^2} = (r - r_c)^2 \left( r^2 + 2r_c r - \frac{a^2 \eta_c}{r_c^2} - \frac{4Q^2 \Delta(r_c)}{(r_c - M)^2} \right). \quad (125)$$

Define  $x = \frac{1}{r - r_c}$ , one can also obtain the expression (108) with a different  $c = 3r_c^2 - \frac{a^2 \eta_c}{r_c^2} - \frac{4Q^2 \Delta(r_c)}{(r_c - M)^2}$ . Figure 11 illustrates the solution of critical orbits with a double root for different values of  $Q$  in the Kerr-Newman background.

## B. Timelike worldline

For timelike critical orbits, the difficulty of analytical calculations increases rapidly. Due to the additional parameters, the expressions involved in analytical computations become highly complex. We begin by examining the case of a triple root. Directly solving the system of equations  $R = 0, R' = 0$ , and  $R'' = 0$  is difficult. We can only solve each equation individually. One can rewrite  $R'' = 0$  as

$$6r^2 - 6(\tilde{e}Q\chi - M\chi^2 + M)r + (a^2 - \eta - \xi^2 + Q^2(\tilde{e}^2 - \chi^2 + 1)) = 0, \quad (126)$$

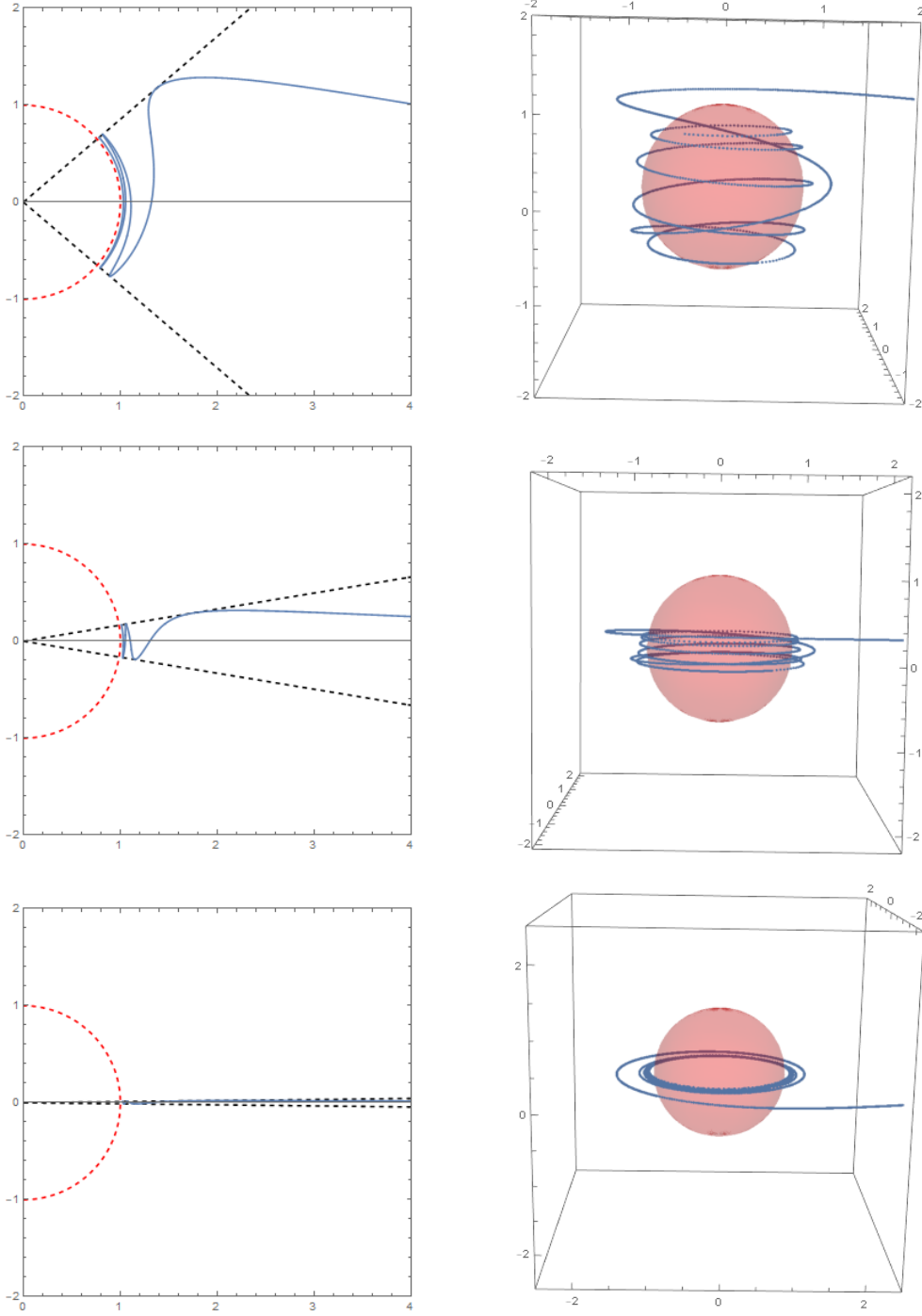


FIG. 10. The critical null geodesics of triple coincident roots in Kerr-Newmann spacetime. The left diagram illustrates the trajectory of a timelike geodesic in the  $(r, \theta)$  plane, while the right diagram shows the trajectory in three-dimensional space. The Mass of the black hole is chosen to be  $M = 1$  and the initial conditions are chosen to be  $r_i = 10, \mu_i = 0, \varphi_i = 0$ . The parameters for each row of images, from top to bottom, are  $Q = 0.5, Q = 0.86, Q = 0.866$ . The red dashed line (ball) is located at  $r = r_c$  and the black dashed line is  $\mu = \pm\mu_m$ .

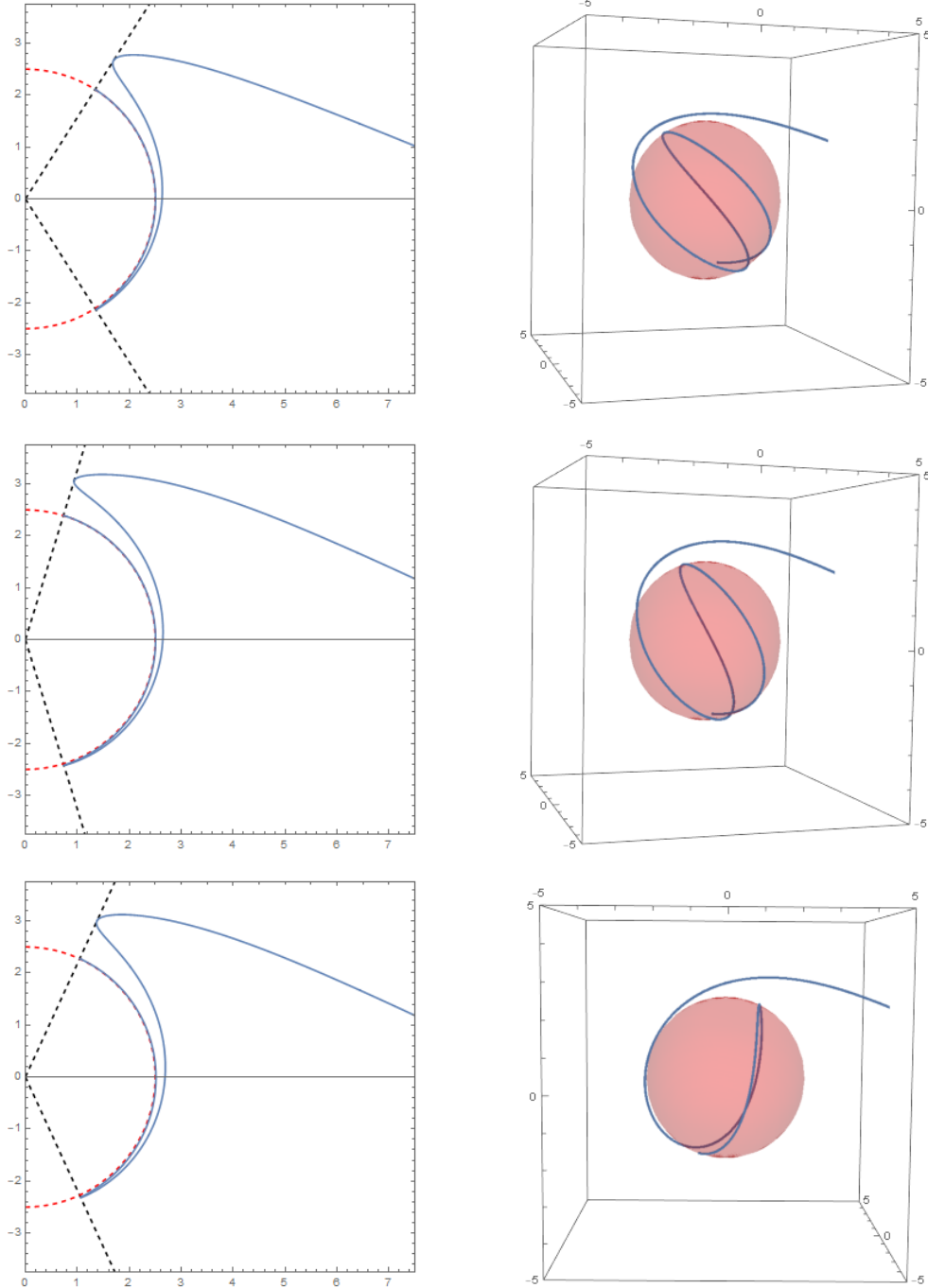


FIG. 11. The critical null orbits of double coincident roots in Kerr-Newman spacetime. The left diagram illustrates the trajectory of null geodesic in the  $(r, \theta)$  plane, while the right diagram shows the trajectory of null geodesic in three-dimensional space. The Mass of the black hole is chosen to be  $M = 1$  and the initial conditions are chosen to be  $r_i = 10, \mu_i = 0, \varphi_i = 0$ . The parameters for each row of images, from top to bottom, are  $Q = 0.3, Q = 0.5, Q = 0.866$  with  $a = 0.5, r_c = 2.5$ . The red dashed line (ball) is located at  $r = r_c$  and the black dashed line is  $\mu = \pm \mu_m$ .

and obtains

$$\eta_c^* = 6r_c^2 + (-6\tilde{e}Q\chi + 6M\chi^2 - 6M)r_c + (a^2 + \tilde{e}^2Q^2 - \xi^2 - Q^2\chi^2 + Q^2). \quad (127)$$

Eliminating  $\eta$  in  $R' = 0$ , one obtains

$$\begin{aligned} & (-a^2\tilde{e}Q\chi + a^2M\chi^2 + a^2M + \tilde{e}^2MQ^2 - MQ^2\chi^2 + MQ^2) + r_c(-6\tilde{e}MQ\chi + 6M^2\chi^2 - 6M^2) \\ & + r_c^2(3\tilde{e}Q\chi - 3M\chi^2 + 9M) - 4r_c^3 + \xi(a\tilde{e}Q - 2aM\chi) = 0. \end{aligned} \quad (128)$$

Thus, we obtain

$$\begin{aligned} \xi_c^* = \frac{1}{a(\tilde{e}Q - 2M\chi)} & \left( (a^2\tilde{e}Q\chi + a^2(-M)\chi^2 - a^2M - \tilde{e}^2MQ^2 + MQ^2\chi^2 - MQ^2) \right. \\ & \left. + r_c(6\tilde{e}MQ\chi - 6M^2\chi^2 + 6M^2) + r_c^2(-3\tilde{e}Q\chi + 3M\chi^2 - 9M) + 4r_c^3 \right). \end{aligned} \quad (129)$$

Eliminating  $\xi$  and  $\eta$  in equation  $R = 0$ , we obtain a quartic algebraic equation in  $\chi$

$$a_0 + a_1\chi + a_2\chi^2 + a_3\chi^3 + a_4\chi^4 = 0, \quad (130)$$

where the coefficients  $a_0 - a_4$  are list in Appendix B. Theoretically, by solving the above equation (130), a complete set of parameters  $\eta = \eta_c^*$ ,  $\xi = \xi_c^*$ , and  $\chi = \chi_c^*$  can be obtained such that the equation  $R = 0$  has a triple root. However, due to the complexity of the coefficients  $a_0 - a_4$ , it is almost impossible to derive an explicit expression for  $\chi = \chi_c^*$ . It is also difficult to determine which parameters satisfy the physical conditions.

Fortunately, we can adopt an alternative approach to discuss the triple root scenario. Actually, we know that the function  $R$  can always be degenerate to

$$\frac{R}{E^2 - m^2} = (r - r_c)^3(r - r_1). \quad (131)$$

Comparing with expression (117), it can be seen that  $r_1 = 2\tilde{e}Q\chi_c^* - 2M\chi_c^{*2} + 2M - 3r_c$ , where  $\chi = \chi_c^*$  satisfies Eq. (130). The integration gives

$$\frac{1}{\sqrt{E^2 - m^2}} \int \frac{dr}{\sqrt{R}} = -\frac{2}{r_c - r_1} \sqrt{\frac{r - r_1}{r - r_c}} + C. \quad (132)$$

It is worth noting that for this scenario to occur, the parameters must still satisfy reasonable conditions, including: (1) the existence of the black hole horizon; (2)  $r_c$  lies outside the horizon; (3)  $\chi > 1$ ; (4)  $r_1 < r_c$ ; (5)  $\eta \geq 0$ , and so on. We have not found a completely reasonable set of parameter values, although we cannot completely rule out the possibility.

The case of double roots is similar to this situation. The expressions for the solutions  $\eta = \eta_c$ ,  $\xi = \xi_c$  that satisfy the conditions  $R = 0$  and  $R' = 0$  are extremely complex, and we will not list them here. The function  $R$  degenerates into

$$\frac{R}{E^2 - m^2} = (r - r_c)^2 \left( r^2 + 2(r_c + M(\chi^2 - 1) - \tilde{e}Q\chi)r + \frac{Q^2(2a\xi_c\chi - a^2\chi^2 - \eta_c - \xi_c^2) - a^2\eta_c}{r_c^2} \right). \quad (133)$$

The integral  $\int \frac{dr}{\sqrt{E^2 - m^2}\sqrt{R}}$  retains the form (113), albeit with different values for  $b$  and  $c$ :

$$b = 2r_c + M(\chi^2 - 1) - \tilde{e}Q\chi, \quad (134)$$

$$c = 3r_c^2 + r_c(M(\chi^2 - 1) - \tilde{e}Q\chi) + \frac{Q^2(2a\xi_c\chi - a^2\chi^2 - \eta_c - \xi_c^2) - a^2\eta_c}{r_c^2}. \quad (135)$$

The numerical results are shown in Fig. 12.

## VII. CONCLUSIONS AND DISCUSSION

When a test particle moves from infinity toward a black hole, those orbits that neither fall into the black hole nor are scattered by it are referred to as critical orbits. This corresponds to the radial kinetic energy  $R(r) = 0$  having either a double or a triple real root. This paper investigates all possible cases of critical orbits, including their motion in four different black hole background spacetimes and for three types of particles (massless particles, massive uncharged particles, and massive charged particles).

In spherically symmetric spacetimes, due to the conservation of angular momentum, orbits are confined to a single plane. For critical orbits in the equatorial plane, the relationship between the radius  $r$  and the angle  $\varphi$  can be expressed analytically. In axisymmetric spacetimes, however, the conserved quantity shifts from angular momentum to the Carter constant, and general orbits exist in three-dimensional space. In the  $\theta$ -direction, the orbit oscillates back and forth around the equatorial plane. We provide the analytical expressions for  $(r, \theta, \varphi)$  and present the corresponding numerical results.

For null geodesics, the critical orbit lies at the boundary of the accreting light rays. Therefore, its shape determines the appearance of the black hole as seen from infinity. For a Schwarzschild black hole, it is a circle with a radius of  $3\sqrt{3}M$ . If the black hole is charged, this radius decreases. Furthermore, as the spin parameter  $a$  increases, the shape gradually becomes D-shaped.

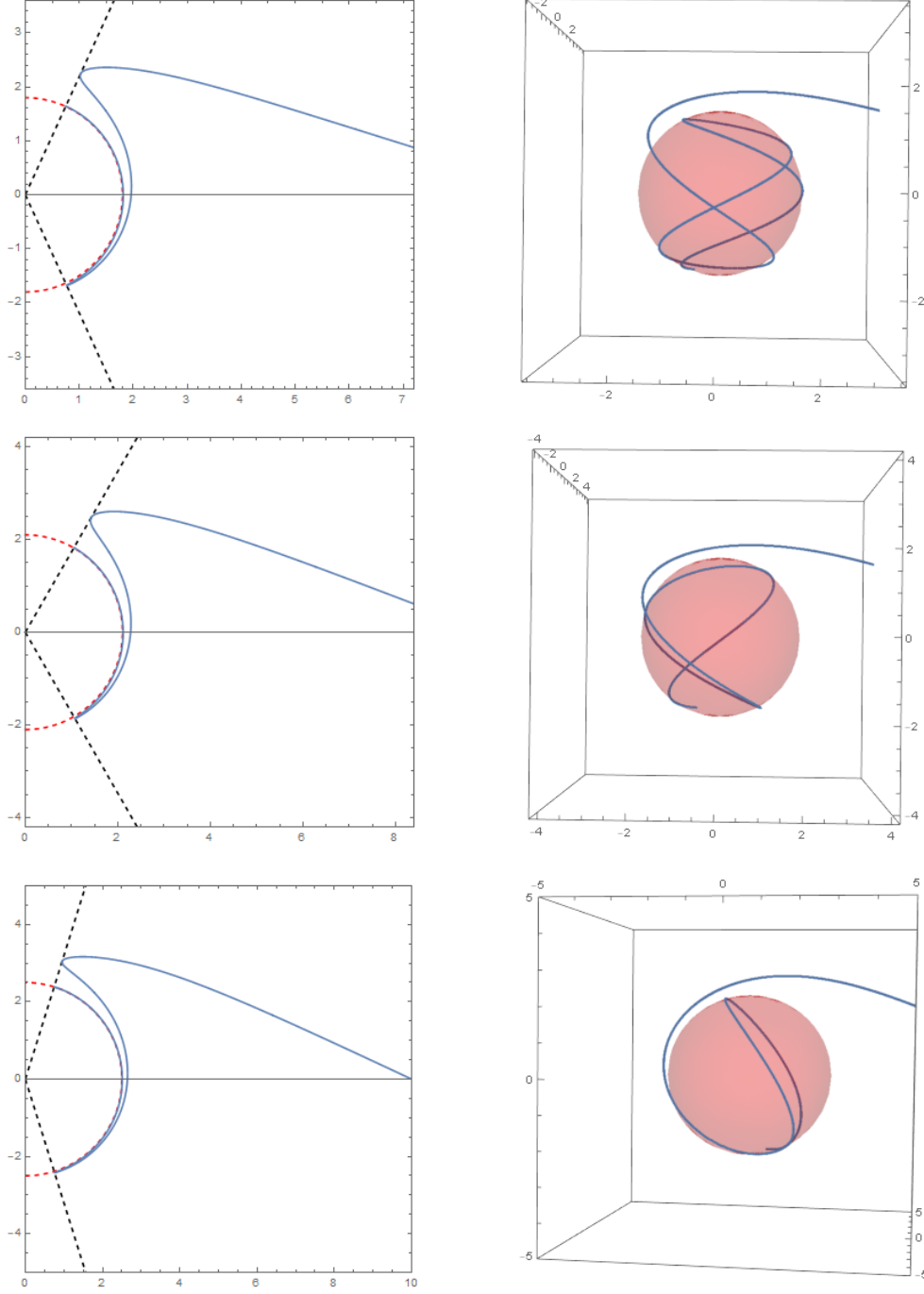


FIG. 12. The critical timelike orbits of double coincident roots in Kerr-Newman spacetime. The left diagram illustrates the trajectory of null geodesic in the  $(r, \theta)$  plane, while the right diagram shows the trajectory of null geodesic in three-dimensional space. The initial conditions are chosen to be  $r_i = 10, \mu_i = 0, \varphi_i = 0$ . The parameters for each row of images, from top to bottom, are  $a = 0.8, r_c = 1.8, Q = 0.5, \tilde{e} = 1.1, \chi = 1.1$ ;  $a = 0.8, r_c = 2.1, Q = 0.3, \tilde{e} = 1.3, \chi = 1.3$ ;  $a = 0.4, r_c = 2.5, Q = 0.6, \tilde{e} = 1.5, \chi = 1.5$ .

In addition, we provide a detailed discussion of the explicit relationships between the physical parameters and the critical radius, which is crucial for the accretion model of collisionless Vlasov gas onto black holes. In the future, we will build a more general theory of black hole accretion based on this work.

## APPENDIX A: THE CRITICAL TIMELIKE GEODESICS WITH TRIPLE ROOTS IN KERR BACKGROUND

The triple roots require  $R = 0$ ,  $R' = 0$  and  $R'' = 0$ , which shows

$$r^4 + 2M(\chi^2 - 1)r^3 + (a^2 - \xi^2 - \eta)r^2 + 2M[\eta + (\xi - a\chi)^2]r - a^2\eta = 0, \quad (136)$$

$$2r^3 + 3M(\chi^2 - 1)r^2 + (a^2 - \xi^2 - \eta)r + M[\eta + (\xi - a\chi)^2] = 0, \quad (137)$$

$$6r^2 + 6M(\chi^2 - 1)r + (a^2 - \xi^2 - \eta) = 0. \quad (138)$$

Solving Eq. (138), one obtains

$$\eta_c^* = a^2 - \xi_c^2 + 6r_c^2 + 6M(\chi_c^2 - 1)r_c. \quad (139)$$

Inserting the solution into Eq. (137), one have

$$a^2M\chi_c^2 + a^2M + 6M^2r_c\chi_c^2 - 6M^2r_c - 3Mr_c^2\chi_c^2 + 9Mr_c^2 - 4r_c^3 - 2\xi_c aM\chi_c = 0. \quad (140)$$

Then, the solution of  $\xi_c$  is given by

$$\xi_c^* = \frac{a^2M\chi_c^2 + a^2M + 6M^2r_c\chi_c^2 - 6M^2r_c - 3Mr_c^2\chi_c^2 + 9Mr_c^2 - 4r_c^3}{2aM\chi_c}. \quad (141)$$

Inserting expressions (139) and (141) into  $R$  and defining

$$A = (a^2M - r_c(6M^2 - 9Mr_c + 4r_c^2))^2, \quad (142)$$

$$B = a^4M + 2a^2r_c(-6M^2 + 3Mr_c + 2r_c^2) + r_c^2(36M^3 - 68M^2r_c + 45Mr_c^2 - 12r_c^3), \quad (143)$$

$$C = a^4 - 6a^2r_c(2M + r_c) + r_c^2(36M^2 - 28Mr_c + 9r_c^2), \quad (144)$$

we can reexpress  $R = 0$  as

$$\frac{1}{4M^2\chi_c^2}(M^2C\chi_c^4 - 2MB\chi_c^2 + A) = 0. \quad (145)$$

Thus, we have

$$\chi_c^2 = \frac{B \pm \sqrt{B^2 - AC}}{MC}, \quad (146)$$

where  $B^2 - AC = 16Mr_c^3\Delta^3(r_c)$ . On the interval  $r_c \in [r_+, \infty)$ , the function  $f(r_c) = B + \sqrt{B^2 - AC}$  is monotonically decreasing, while  $C(r_c)$  is monotonically increasing. It can be shown that for  $a \in [0, M]$ ,  $f(r_+) \leq 0$  and  $C(r_+) \geq 0$ . Consequently, for  $r_c > r_+$ , we have  $\chi_c^2 < 0$ . Therefore, no physically allowed parameter range exists.

## APPENDIX B: THE COEFFICIENTS $a_0$ - $a_4$

$$\begin{aligned}
a_0 = & a^2 \left( (a^2 + (\tilde{e}^2 + 1) Q^2) (a^2(\tilde{e}Q + M)(M - \tilde{e}Q) + (\tilde{e}^2 + 1) M^2 Q^2 - \tilde{e}^2 Q^4) \right. \\
& + 6r_c(a^2(\tilde{e}^2 M Q^2 - 2M^3) - 2(\tilde{e}^2 + 1) M^3 Q^2 + \tilde{e}^2 M Q^4) - 6r_c^2(a^2(\tilde{e}^2 Q^2 - 3M^2) \\
& - 3(\tilde{e}^2 + 1) M^2 Q^2 + \tilde{e}^2 Q^4 - 6M^4) - 2r_c^3(M(4a^2 + (5\tilde{e}^2 + 4) Q^2 + 54M^2)) \\
& \left. + 3r_c^4(\tilde{e}^2 Q^2 + 43M^2) - 72Mr_c^5 + 16r_c^6 \right), \tag{147}
\end{aligned}$$

$$\begin{aligned}
a_1 = & a^2 \tilde{e}Q \left( 2M(a^2 + Q^2)(a^2 + (\tilde{e}^2 + 1) Q^2) + 6r_c(-2(2 + en^2)M^2 Q^2 + en^2 Q^4 \right. \\
& + a^2(-4M^2 + en^2 Q^2)) + 6Mr_c^2(2a^2 + (\tilde{e}^2 + 2) Q^2 + 12M^2) + r_c^3(8a^2 - 2(\tilde{e}^2 - 4) Q^2 \\
& \left. - 136M^2) + 90Mr_c^4 - 24r_c^5 \right), \tag{148}
\end{aligned}$$

$$\begin{aligned}
a_2 = & a^2 \left( (a^2 + Q^2) (a^2(\tilde{e}^2 Q^2 - 2M^2) - 2(\tilde{e}^2 + 1) M^2 Q^2 + \tilde{e}^2 Q^4) \right. \\
& + 6r_c(a^2(4M^3 - 3\tilde{e}^2 M Q^2) + 2(\tilde{e}^2 + 2) M^3 Q^2 - 3\tilde{e}^2 M Q^4) \\
& + r_c^2(-6a^2(\tilde{e}^2 Q^2 + 2M^2) + 6(5\tilde{e}^2 - 2) M^2 Q^2 - 6\tilde{e}^2 Q^4 - 72M^4) \\
& \left. + r_c^3(-8a^2 M - 2(13\tilde{e}^2 + 4) M Q^2 + 136M^3) + r_c^4(9\tilde{e}^2 Q^2 - 90M^2) + 24Mr_c^5 \right), \tag{149}
\end{aligned}$$

$$\begin{aligned}
a_3 = & 2Ma^2 \tilde{e}Q \left( -(a^2 + Q^2)^2 + 12M(a^2 + Q^2)r_c + 6r_c^2(a^2 - 6M^2 + Q^2) + 28Mr_c^3 - 9r_c^4 \right), \tag{150}
\end{aligned}$$

$$\begin{aligned}
a_4 = & M^2 a^2 \left( (a^2 + Q^2)^2 - 12r_c(M(a^2 + Q^2)) - 6r_c^2(a^2 - 6M^2 + Q^2) - 28Mr_c^3 + 9r_c^4 \right). \tag{151}
\end{aligned}$$

**Acknowledgement** This work is partially supported by National Natural Science Foundation of China (Grant No.12505071) and by the Research Foundation of Education Bureau

of Hunan Province, China (Grant No. 25B0635). This work is also partially supported by Hunan Provincial Department of Education Key Laboratory of Information Detection and Intelligent Processing Technology, and by Applied Characteristic Subject of Hunan Province "Electronic Science and Technology".

---

- [1] J. Droste, The Field of a Single Centre in Einstein's Theory of Gravitation, and the Motion of a Particle in That Field, *Huygens Institute - Royal Netherlands Academy of Arts and Sciences (KNAW)* 197-215; "Golden Oldie": The Field of a Single Centre in Einstein's Theory of Gravitation, and the Motion of a Particle in That Field, *Gen. Relativ. Gravit.* **34**, 1545-1563 (2002).
- [2] Y. Hagihara, Theory of the Relativistic Trajectories in a Gravitational Field of Schwarzschild, *Japanese Journal of Astronomy and Geophysics* **8**, 67-176 (1931).
- [3] S. Grunau and V. Kagramanova, Geodesics of electrically and magnetically charged test particles in the Reissner-Nordström space-time: analytical solutions, *Phys. Rev. D* **83**, 044009 (2011).
- [4] A. R. Forsyth, Note on the central differential equation in the relativity theory of gravitation, *Proc. R. Soc. Lond. A* **97**, 145-151 (1920).
- [5] A. G. Greenhill, Newton-Einstein planetary orbits, *The London, Edinburgh, and Dublin Philosophical Magazine and Journal of Science* **41**, 143 (1921).
- [6] C.G. Darwin, The gravity field of a particle, *Proc. R. Soc. Lond. A* **249**, 180-194.
- [7] C.G. Darwin, The gravity field of a particle II, *Proc. R. Soc. Lond. A* **263**, 39-50.
- [8] C. M. Rodríguez, Orbits in general relativity: The Jacobian elliptic functions, *Nuov. Cim. B*, **98**, 87-96 (1987).
- [9] G. Scharf, Schwarzschild Geodesics in terms of Elliptic functions and the related red shift, *J. Mod. Phys* **2**, 274-283.
- [10] B. Carter, Global structure of Kerr family of gravitational fields, *Phys. Rev.* **174**, 1559 (1968).
- [11] Y. Mino, Perturbative approach to an orbital evolution around a supermassive black hole, *Phys. Rev. D* **67**, 084027 (2003).
- [12] R. Fujita and W. Hikida, Analytical solutions of timelike geodesic orbits in Kerr spacetime geodesic orbits in Kerr spacetime, *Classical Quantum Gravity* **26**, 135002 (2009).

- [13] S. E. Gralla and A. Lupsasca, Null geodesics of the Kerr exterior, *Phys. Rev. D* **101**, 044032 (2020).
- [14] Chen-Yu Wang, Da-Shin Lee and Chi-Yong Lin, Geodesic motion of neutral particles around a Kerr-Newman black hole, *Classical Quantum Gravity* **34**, 235008 (2017)
- [15] Chen-Yu Wang, Da-Shin Lee and Chi-Yong Lin, Null and timelike geodesics in the Kerr-Newman Black hole exterior, *Phys. Rev. D* **106**, 084048 (2022).
- [16] D. V. Galtsov and K. V. Kobialko, Completing characterization of photon orbits in Kerr and Kerr-Newman metrics, *Phys. Rev. D* **99**, 084043 (2019).
- [17] Bo-Ruei Chen, Tien Hsieh and Da-Shin Lee, Null geodesics in extremal Kerr-Newman black holes, *Phys. Rev. D* **111**, 024058 (2025).
- [18] E. Hackmann and C. Lämmerzahl, Complete Analytic Solution of the Geodesic Equation in Schwarzschild- (Anti-) de Sitter Spacetimes, *Phys. Rev. Lett.* **100**, 171108 (2008).
- [19] E. Hackmann and C. Lämmerzahl, Geodesic equation in Schwarzschild- (anti-) de Sitter spacetimes: Analytical solutions and applications, *Phys. Rev. D* **78**, 024035 (2008).
- [20] E. Hackmann and C. Lämmerzahl, Analytic solutions of the geodesic equation in higher dimensional static spherically symmetric space-times, *Phys. Rev. D* **78**, 124018 (2008).
- [21] E. Hackmann, C. Lämmerzahl, V. Kagramanova and J. Kunz, Analytical solution of the geodesic equation in Kerr-(anti) de Sitter space-times, *Phys. Rev. D* **81**, 044020 (2008).
- [22] J. M. Bardeen, Timelike and null geodesics in the Kerr metric, in *Black Holes* (Les astres Occlus), edited by C. Dewitt and B. S. Dewitt (Gordon and Breach Science Publishers, New York, 1973), pp 215-283.
- [23] S. Chandrasekhar, *The Mathematical Theory of Black Holes* (Clarendon Press, Oxford, 1983).
- [24] B. O'Neill, *The Geometry of Kerr Black Holes* (A K Peters, Ltd., Natick, Massachusetts, 1995).
- [25] C. Lammerzahl and E. Hackmann, Analytical solutions for geodesic equation in black hole spacetimes, *Springer Proc. Phys.* **170**, 43 (2016).
- [26] P. Rioseco and O. Sarbach, Accretion of a relativistic, collisionless kinetic gas into a Schwarzschild black hole, *Classical Quantum Gravity* **34**, 095007 (2017).
- [27] P. Rioseco and O. Sarbach, Spherical steady-state accretion of a relativistic collisionless gas into a Schwarzschild black hole, *J. Phys. Conf. Ser.* **831**, 012009 (2017).
- [28] P. Mach and A. Odrzywołek, Accretion of Dark Matter onto a Moving Schwarzschild Black

- Hole: An Exact Solution, *Phys. Rev. Lett.* **126**, 101104 (2021).
- [29] P. Mach and A. Odrzywołek, Accretion of the relativistic Vlasov gas onto a moving Schwarzschild black hole: Exact solutions, *Phys. Rev. D* **103**, 024044 (2021).
- [30] A. Cieřlik and P. Mach, Accretion of the Vlasov gas on Reissner-Nordström black holes, *Phys. Rev. D* **102**, 024032 (2020).
- [31] Ping Li, Yong-qiang Liu and Xiang-hua Zhai, Accretion of the relativistic Vlasov gas onto a Kerr black hole, *Phys. Rev. D* **108**, 124022 (2023).
- [32] Patryk Mach, Mehrab Momennia, Olivier Sarbach, Accretion of a Vlasov gas by a Kerr black hole, arXiv: 2508.04783.
- [33] Patryk Mach, Mehrab Momennia, Olivier Sarbach, Bondi-type accretion onto a Kerr black hole in the kinetic regime, arXiv: 2508.20189.
- [34] P. Mach, A. Cieřlik and A. Odrzywołek, Monte Carlo methods for stationary solutions of general-relativistic Vlasov systems: Collisionless accretion onto black holes, *Phys. Rev. D* **108**, 124057 (2023).
- [35] A. Cieřlik, P. Mach and A. Odrzywołek, Monte Carlo methods for stationary solutions of general-relativistic Vlasov systems: Planar accretion onto a moving Schwarzschild black hole, *Phys. Rev. D* **110**, 084014 (2024).
- [36] Adam Cieřlik, Patryk Mach, Revisiting timelike and null geodesics in the Schwarzschild space-time: general expressions in terms of Weierstrass elliptic functions, *Classical Quantum Gravity* **39**, 225003 (2022).
- [37] Adam Cieřlik, Patryk Mach, Timelike and null geodesics in the Schwarzschild space-time: Analytical solutions, *Acta Phys. Polon. Supp.* **16** 6-A10 (2023).
- [38] Ping Li, Jiang-he Yang and Siwei Xu, Accretion of the degenerate Fermi gas onto a Reissner-Nordström black hole, *Physics Letters B*, **866** 139555 (2025).